THE JOURNAL OF COMPARATIVE NEUROLOGY 502:522–543 (2007)

Ultrastructural Analysis of Aminoglycoside-Induced Hair Cell Death in the Zebrafish Lateral Line Reveals an Early Mitochondrial Response

KELLY N. OWENS,[1–3]* DALE E. CUNNINGHAM,[2,3] GLEN MACDONALD,[2,3] EDWIN W. RUBEL,[2,3] DAVID W. RAIBLE,[1,2] AND REMY PUJOL[2–4]

[1]Department of Biological Structure, University of Washington, Seattle, Washington 98195
[2]Virginia Merrill Bloedel Hearing Research Center, University of Washington, Seattle, Washington 98195
[3]Department of Otolaryngology-Head and Neck Surgery, University of Washington, Seattle, Washington 98195
[4]INSERM Unit 583, Université Montpellier, INM, Hôpital St. Eloi, BP 74103, Montpellier, 34090 France

ABSTRACT

Loss of the mechanosensory hair cells in the auditory and vestibular organs leads to hearing and balance deficits. To investigate initial, in vivo events in aminoglycoside-induced hair cell damage, we examined hair cells from the lateral line of the zebrafish, *Danio rerio*. The mechanosensory lateral line is located externally on the animal and therefore allows direct manipulation and observation of hair cells. Labeling with vital dyes revealed a rapid response of hair cells to the aminoglycoside neomycin. Similarly, ultrastructural analysis revealed structural alteration among hair cells within 15 minutes of neomycin exposure. Animals exposed to a low, 25-μM concentration of neomycin exhibited hair cells with swollen mitochondria, but little other damage. Animals treated with higher concentrations of neomycin (50–200 μM) had more severe and heterogeneous cellular changes, as well as fewer hair cells. Both necrotic-like and apoptotic-like cellular damage were observed. Quantitation of the types of alterations observed indicated that mitochondrial defects appear earlier and more predominantly than other structural alterations. In vivo monitoring demonstrated that mitochondrial potential decreased following neomycin treatment. These results indicate that perturbation of the mitochondrion is an early, central event in aminoglycoside-induced damage. J. Comp. Neurol. 502:522–543, 2007.

Indexing terms: ototoxicity; mechanosensation; neomycin; neuromast; mitochondria; transmission electron microscopy

The majority of permanent hearing and balance disorders are due to death of hair cells, the mechanosensory cells of the auditory and vestibular sensory systems. Death of hair cells can arise from a multitude of causes, including exposure to toxic agents, noise trauma, and aging. The relationship between hair cell death from iatrogenic damage, noise-induced hearing loss, and age-related hearing loss is not well understood. Of these forms of hair cell loss, drug exposure is the most easily manipulable in the laboratory setting.

Aminoglycosides are antibiotics that act against Gram-negative bacteria and mycoplasmas (Vakulenko and Mobashery, 2003). Shortly after its identification and initial clinical use, the aminoglycoside streptomycin was recognized to be cochleotoxic, vestibulotoxic, and nephrotoxic

Grant sponsor: National Institute on Deafness and Other Communication Disorders (NIDCD); Grant numbers: DC05987, DC06998, DC04661; Grant sponsor: Virginia Merrill Bloedel Hearing Research Center.

*Correspondence to: Kelly N. Owens, VM Bloedel Hearing Research Center, Box 357923, University of Washington, Seattle, WA 98195.
E-mail: kowens@u.washington.edu

Received 2 May 2006; Revised 6 November 2006; Accepted 25 January 2007
DOI 10.1002/cne.21345
Published online in Wiley InterScience (www.interscience.wiley.com).

(Hinshaw and Feldman, 1945; reviewed in Forge and Schacht, 2000). Efforts to identify alternative aminoglycosides demonstrated similar toxicity of other drugs among this chemical class. These antibiotics remain in use in the US for treatment of recalcitrant bacterial infections (e.g., among premature infants, cystic fibrosis, or HIV patients) and are among the most commonly prescribed drugs in developing countries due to their efficacy and relatively low expense (Forge and Schacht, 2000).

The mechanism underlying toxicity of aminoglycosides in eukaryotes is not well understood. The bactericidal activity of aminoglycosides occurs by interference with bacterial translation (Davies, 1965). Specifically, aminoglycosides bind the 16S ribosomal subunit, altering its conformation at the A-site and disrupting codon–anticodon interaction, and thus disrupt the fidelity of the translation process (Vicens and Westof, 2003). Divergence of the analogous component in the eukaryotic ribosome is thought to prevent inhibition of translation by aminoglycosides (Wilhelm et al., 1978; Recht et al., 1999). However, the eukaryotic mitochondrial ribosome more closely resembles the prokaryotic ribosome (Gutell et al., 1994) and may share its aminoglycoside sensitivity. Aminoglycosides have also been postulated to target other intracellular processes including lipid metabolism, actin cytoskeleton and lysosome function, and/or mitochondrial ATP production (Akiyoshoi et al., 1976; Kossl et al., 1990; Pickles and Rouse 1991; Hashino et al., 1997). How toxicity is limited to, or enhanced in, particular tissue types (namely, mechanosensory and kidney cells) remains unclear.

The process of aminoglycoside-induced cell death has been examined in the mammalian and avian inner ear by scanning electron microscopy (SEM) and transmission electron microscopy (TEM) following chronic systemic injection of aminoglycosides. A constellation of phenotypes occurs, including swollen hair cells, nuclear shrinkage, mitochondrial dilation, stereocilia fusion, accumulation of granular cytoplasmic contents, increase of dense lysosomal vesicles and myeloid bodies, and cell extrusion/evulsion (Wersall and Hawkins, 1962; Ylikoski, 1974; Weisleder and Rubel, 1992). The majority of early studies were done using a multi-day course of treatment followed by varying survival times prior to examination. While these studies clearly demonstrated the ability of aminoglycosides to induce damage, it remained unclear which cellular events were primary effects and which were sequelae of aminoglycoside-induced damage.

The development of protocols using single injections of aminoglycosides and alternative modes of administration (namely, intratympanic injection or pledget use versus subcutaneous or intramuscular injection; e.g., Janas et al., 1995) allowed more direct temporal evaluation. Much attention has been given to defining the extent of damage and, in avians, the onset of regeneration. However, few studies report the initial cellular events that occur in response to aminoglycosides. Hirose et al. (2004) examined the chick basilar papilla, the avian auditory organ, at short intervals following a single, large aminoglycoside injection. At 8–12 hours after the injection, hair cells appeared rounded and swollen, with condensation of nuclear chromatin, dissolution of ribosomes, and dilation of mitochondria, and increased numbers of inclusion bodies and lysosomes. With increasing time, progressively more severe degeneration occurred. In contrast to in vivo work in chick and guinea pig, in vitro vestibular or cochlear hair cells exhibit relatively rapid responses to aminoglycosides (Sobkowicz et al., 1975; Kossl et al., 1990; Forge and Richardson, 1993; Hirose et al., 1997; Dehne et al., 2002).

In vivo studies of hair cell toxicity in mammalian and avian inner ears are limited by the relative inaccessibility of mechanosensory cells, which are embedded within the temporal bone. Administration of aminoglycosides systemically or by injection into the cochlea makes it difficult to ascertain the dose of drug reaching the hair cell (Tran Ba Huy, 1981). Furthermore, the first time of examination after drug exposure has usually been hours or days after drug exposure. To circumvent these limitations, we have chosen to use the zebrafish lateral line as a model system for studying aminoglycoside-induced hair cell death. The zebrafish lends itself to genetic analyses and in vivo manipulation. In addition, it is getting increasing attention as a vertebrate preparation for studying diseases (e.g., Dooley and Zon, 2000; Dambly-Chaudiere et al., 2003), including auditory dysfunction (reviewed in Nicolson et al., 2005), metal toxicity (Hernandez et al., 2006), and aminoglycoside-induced renal damage (Hentschel et al., 2005).

The lateral line of zebrafish, like that of other fish and aquatic amphibians, is composed of neuromasts, or clusters of mechanosensory hair cells and support cells, and their innervating lateral line nerves (Leydig, 1850; Metcalfe, 1985; Raible and Kruse, 2000). The lateral line is thought to detect local disturbances in the patterns of current flow as well as the orientation of the animal in the surrounding water current (Dijkgraaf, 1963; Coombs and Montgomery, 1999). The anterior lateral line surrounds the head of the zebrafish, while the posterior lateral line extends along the midline on either side of the animal (Fig. 1A). As in their mammalian and avian counterparts, hair cell death occurs in the lateral line of fish in response to ototoxic agents (Kaus, 1987; Song et al., 1995; Harris et al., 2003). Zebrafish lateral line hair cells respond to neomycin after exposure to drug for 1 hour in a dose-dependent manner, following a period of initial developmental insensitivity (Harris et al., 2003; Murakami et al., 2003; Santos et al., 2006).

In this article we examine aminoglycoside-induced hair cell death in the zebrafish lateral line using ultrastructural analysis to identify the earliest subcellular responses. The external location of hair cells in the lateral line allows direct observation, in vivo, of drug-induced hair cell changes, and thereby the opportunity to correlate ultrastructural changes with dynamic in vivo cellular events. We find that response of lateral line hair cells is rapid, occurring within 15 minutes of drug exposure. We provide quantitative evidence that the initial response involves ultrastructural changes to mitochondria, and these observations are supported by in vivo monitoring of mitochondrial potential. These results suggest that alteration of mitochondrial function has an early, and probably essential, role in aminoglycoside-induced damage.

MATERIALS AND METHODS

Zebrafish larvae (*Danio rerio*) were bred and reared at 28.5°C by standard methods (Westerfield, 1995) in our fish facility according to protocols approved by the University of Washington IACUC. All experiments were performed with the wildtype strain, *AB.

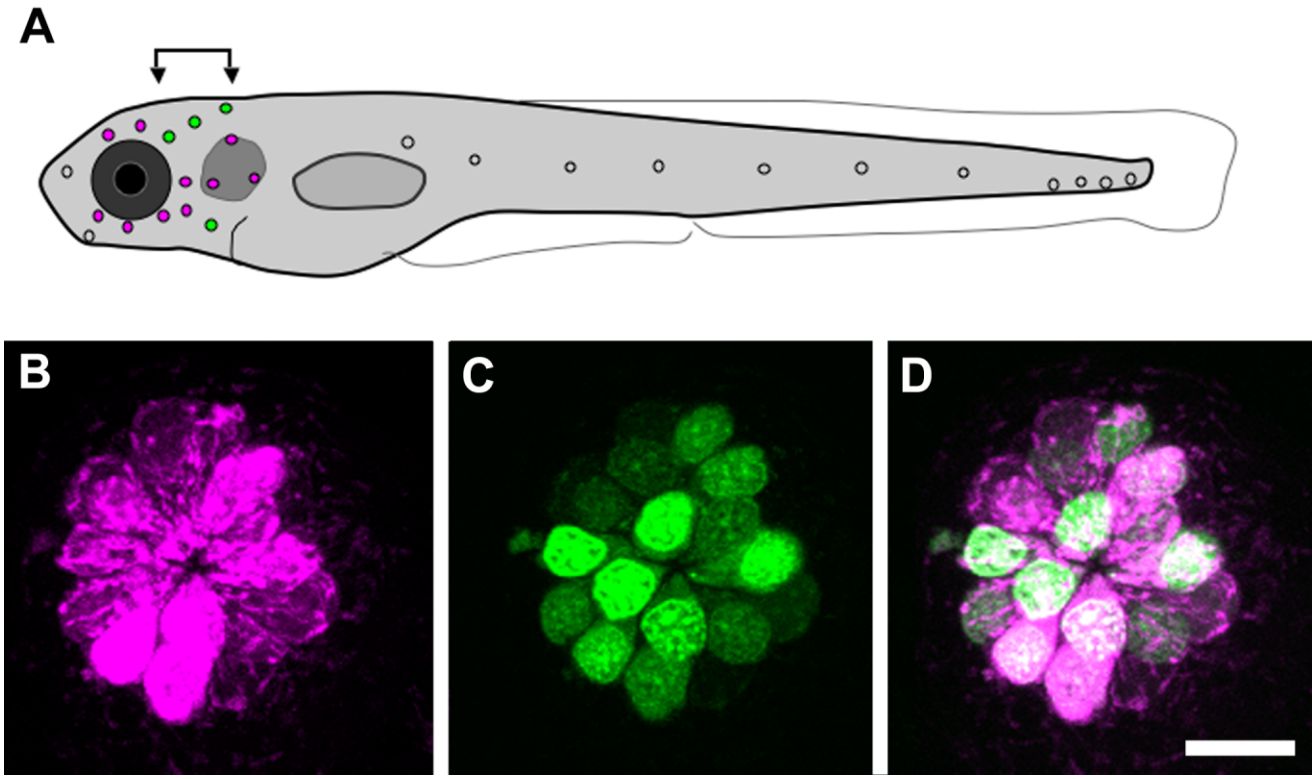

Fig. 1. Neuromasts of wildtype zebrafish lateral line. **A:** Schematic diagram of a 5-day postfertilization (dpf) larva. Location of anterior and posterior lateral line neuromasts are indicated with black circles. The 10 neuromasts examined during DASPEI assays are indicated by magenta fill. Arrows mark the planes at which the majority of transverse sections were taken for ultrastructural analysis (neuromasts typically observed in these sections are indicated in green and magenta). **B–D:** A single neuromast imaged en face showing the hair cells arranged in a rosette. B: DASPEI, a vital mitochondrial dye. C: YO-PRO-1, a vital DNA dye. D: Merged image of B and C. Scale bar = 10 μm.

For neomycin exposure, larvae 5 days postfertilization (dpf) were transferred manually to baskets in 6-well culture plates (Harris et al., 2003) containing defined E2 embryo medium (Westerfield, 1995). All treatment and wash volumes were 6 mL unless otherwise indicated. Larvae were immersed in 0–200 μM neomycin (Sigma-Aldrich, St. Louis, MO, cat. no. N1142) diluted in embryo medium for 15–60 minutes, and subsequently washed rapidly four times in fresh embryo medium. For treatment protocols indicating a recovery period, larvae were held in the final wash of embryo media for the indicated time.

For in vivo assessment of neuromasts, larvae were treated with neomycin for a designated time (see below) and rinsed four times in fresh embryo medium, simultaneous to the preparation of larvae for ultrastructural analysis. Embryos were then immediately stained with DASPEI (0.005% final concentration, 2-{4-(dimethylamino)styryl}-N-ethylpyridinium iodide; Molecular Probes, Eugene, OR) for 15 minutes. DASPEI labels mitochondria, which are abundant in hair cells (e.g., Flock et al., 1997). Following DASPEI labeling, larvae were washed twice with embryo medium and anesthetized with MS222 (3-aminobenzoic acid ethyl ester, methanesulfonate salt; Sigma, St. Louis, MO) diluted in embryo media. DASPEI staining was visualized under epifluorescent illumination using a Nikon dissecting microscope and a DASPEI filter set (Chroma Technologies, Brattleboro, VT) as reported in Harris et al. (2003). Briefly, 10 neuromasts (SO1-2, IO1-4, M2, MI1-2, and O2, shown in magenta in Fig. 1A) were evaluated on each fish for DASPEI staining and were scored (0 for no/little staining, 1 for reduced staining, 2 for full staining). Scores for the 10 neuromasts were totaled to obtain a score (0–20) for each fish. Six to fourteen fish (i.e., 60–140 neuromasts) were evaluated for each dose and treatment group. Analysis of variance (ANOVA) statistics were performed using StatView 5.0 (Cary, NC) software.

For Figure 1, fish were additionally prelabeled for 1 hour with 3 μM YO-PRO-1 (DNA dye, Molecular Probes; excitation 491 nm, emission 509 nm) prior to DASPEI labeling. Optical sections in z-series were collected using a LSM Pascal 5 confocal microscope. For Figure 4, representative in vivo images of DASPEI-labeled IO2 hair cells were obtained on a Zeiss Axioplan 2ie epifluorescent microscope with a cooled CCD camera using a 20× NA 0.75 PlanApo objective. Optical sections were collected with a 50-ms exposure at 1-μm intervals spanning the neuromast using Slidebook 3.0. Sixteen 1-μm sections were stacked in Photoshop 7.0 (Adobe, San Jose, CA) to create a brightest point projection image.

To assess mitochondrial response in vivo, larval hair cell mitochondria were labeled with the mitochondrial potential indicator, Mitotracker Red CMXRos (MTR, Molecular Probes) and/or the mitochondrial mass indicator, Mito-

tracker Green (MTG, Molecular Probes). The ratio between MTR and MTG labeling was assessed to determine the change in mitochondrial potential. Fluorescent indicators were visualized on a Marianas imaging system (Intelligent Imaging Innovations, Denver, CO), consisting of a Zeiss Axiovert 200M inverted compound microscope (Carl Zeiss, Thornwood, NY), 25× NA 0.8 LCI Plan-NeoFluar multi-immersion objective (Zeiss) set for water immersion, a shuttered 175 W xenon lamp coupled by a liquid light guide (Sutter, Novato, CA), and a CoolSnap HQ monochrome cooled CCD camera (Princeton Instruments, Trenton, NJ). The stage and surrounding chamber of the microscope were heated to 28°C prior to and during imaging experiments. Z-stack images of neuromasts were collected. The system was controlled by Slidebook software 4.0.2.1 (Intelligent Imaging) running on a Macintosh G4 computer.

Hair cell mitochondria were labeled by placing 5 dpf zebrafish in 25 nM each of Mitotracker Red (MTR, Molecular Probes) and Mitotracker Green (MTG, Molecular Probes) diluted in embryo medium (hereafter, MTR/MTG). The fish were transferred to medium with fresh MTR/MTG, neomycin (0–50 μM, Sigma N1142) and the anesthetic MS222 (hereafter, MTR/MTG+neo), then transferred along with their medium to an imaging chamber consisting of a 2-chamber coverslip culture chamber with a #1.5 thickness coverslip bottom (Lab-Tek, Naperville, IL) in a drop of minimal volume. The fish were immobilized with an organ culture insert membrane that was wetted with the same MTR/MTG+neo solution. To prevent evaporation during imaging, the second chamber was filled with distilled water and then the cover was set in place. Animal viability was confirmed by monitoring heartbeat.

The fish were oriented so that the SO2 neuromast was as close to orthogonal to the axis of focus as possible and imaged with a minimal number of focal planes. At 5-minute intervals the entire neuromast was imaged in 16–19 image planes at 1-μm intervals. Image capture times were 40–65 ms for MTR and 150 ms for MTG. In all cases exposure times for a given channel were constant throughout the imaging time course. The elapsed time from the placement into MTR/MTG+neo to the capture of the first z-series was 3–5 minutes.

Consistency of the optical system was monitored by measuring the mean intensities of a fluorescent standard recorded using the same filters and exposure times as for the mitochondrial indicators. The images were digitized at 12-bits per pixel upon capture and exported as TIFF files. Datasets were rejected if lateral drift or focal changes prevented the entire neuromast from being analyzed over the entire experimental time. Images were analyzed with ImageJ (Rasband, 1997–2006). An oval region of interest (ROI) was selected to define the margin of the neuromast sensory cells encompassing their basal portion, but excluding the mantle region. All ROIs were recorded with the ImageJ ROI Manager to allow repeat measurements. Integrated intensity was measured within the ROI for all planes and channels at all timepoints. The mean intensity of the ROI was calculated. A thresholded measurement was determined for each slice by measuring the intensities above the nonthresholded mean intensity of the ROI plus 25% of the standard deviation of the nonthresholded mean within the ROI from the initial measurements. The integrated intensity for each image plane was then summed for each timepoint and the change in the ratio of MTR to MTG was calculated as a proportion of the values relative to the initial timepoint of the experiment. Proportional change = (ratio of summed intensities(time point n) – ratio of summed intensities(time point 1)/ratio of summed intensities(time point 1)).

For ultrastructural analysis, larvae were prepared from the same clutch as the in the in vivo DASPEI experiment. Zebrafish larvae were euthanized by immersion in ice-cold embryo medium, fixed in ice-cold 4% glutaraldehyde in 0.1 M sodium cacodylate + 0.001% $CaCl_2$ (pH 7.4, 583 mOsm) for 1 hour at 25°C with gentle agitation, and then with fresh fixative overnight at 4°C. Samples were washed three times for 10 minutes with 0.1 M sodium cacodylate (pH 7.4) + 0.001% $CaCl_2$, postfixed in 1% osmium tetroxide in 0.1 M sodium cacodylate (pH 7.4) + 0.001% $CaCl_2$ for 30 minutes on ice in the dark, with agitation, and then washed 3 × 10 minutes with 0.1 M sodium cacodylate (pH 7.4) + 0.001% $CaCl_2$. Samples were dehydrated in a graded ethanol series (10 minutes each in 35% EtOH, 70% EtOH, 95% EtOH, and twice in 100% EtOH), washed twice for 10 minutes in propylene oxide, once in 1:1 mixture of propylene oxide: Spurr's epoxy resin (Electron Microscopy Sciences, Ft. Washington, PA) for 1 hour, immersed in 100% Spurr's epoxy resin for 1 hour, and placed in fresh 100% Spurr's epoxy resin overnight for infiltration. Fish were embedded in 100% firm Spurr's epoxy resin in silicone rubber molds (Ted Pella, Redding, CA, cat. no. 10504) with zebrafish oriented lengthwise, rostral to caudal. Blocks were baked at 60°C for 18–24 hours. Sections were typically taken just posterior to the eye to allow evaluation of several neuromasts in the same section (indicated by arrows in Fig. 1A, including neuromasts IO3, IO4, M2, MI1, O1, O2, OC1, and/or OP1 using the nomenclature of Raible and Kruse [2000]). Semithin sections (≈2 μm) were cut and stained with 1% Toluidine blue in 1% sodium borate and examined. When a semithin section was observed in which neuromasts were present, ultrathin sections of ≈90 nm were collected on 200 mesh Athene thin-bar grids (Ted Pella). A semithin section was taken between two series of ultrathin sections to allow observation of a different set of hair cells (HCs) from the same neuromasts. Tissue was contrasted with 5% uranyl acetate in 50% methanol for 20 minutes, rinsed with 50% methanol and counterstained with 0.3% lead citrate in 0.1 N NaOH for 4 minutes, then rinsed with distilled water. Samples were examined with a JEOL 1200EXII transmission electron microscope and photographed. Negatives were scanned at 600 dpi to create positive digital images. The entire image was adjusted to optimize the contrast and brightness and cropped. For enumeration of events observed in HCs in Table 1, HCs with one or more swollen mitochondria were counted as containing swollen mitochondria. We define swollen mitochondria in this study as mitochondria that are less electron-dense (increased translucence) than normal with reduced or disordered cristae.

RESULTS

Structure of the zebrafish lateral line hair cells

We examined the cellular events preceding hair cell (HC) death to identify the earliest evidence of drug-

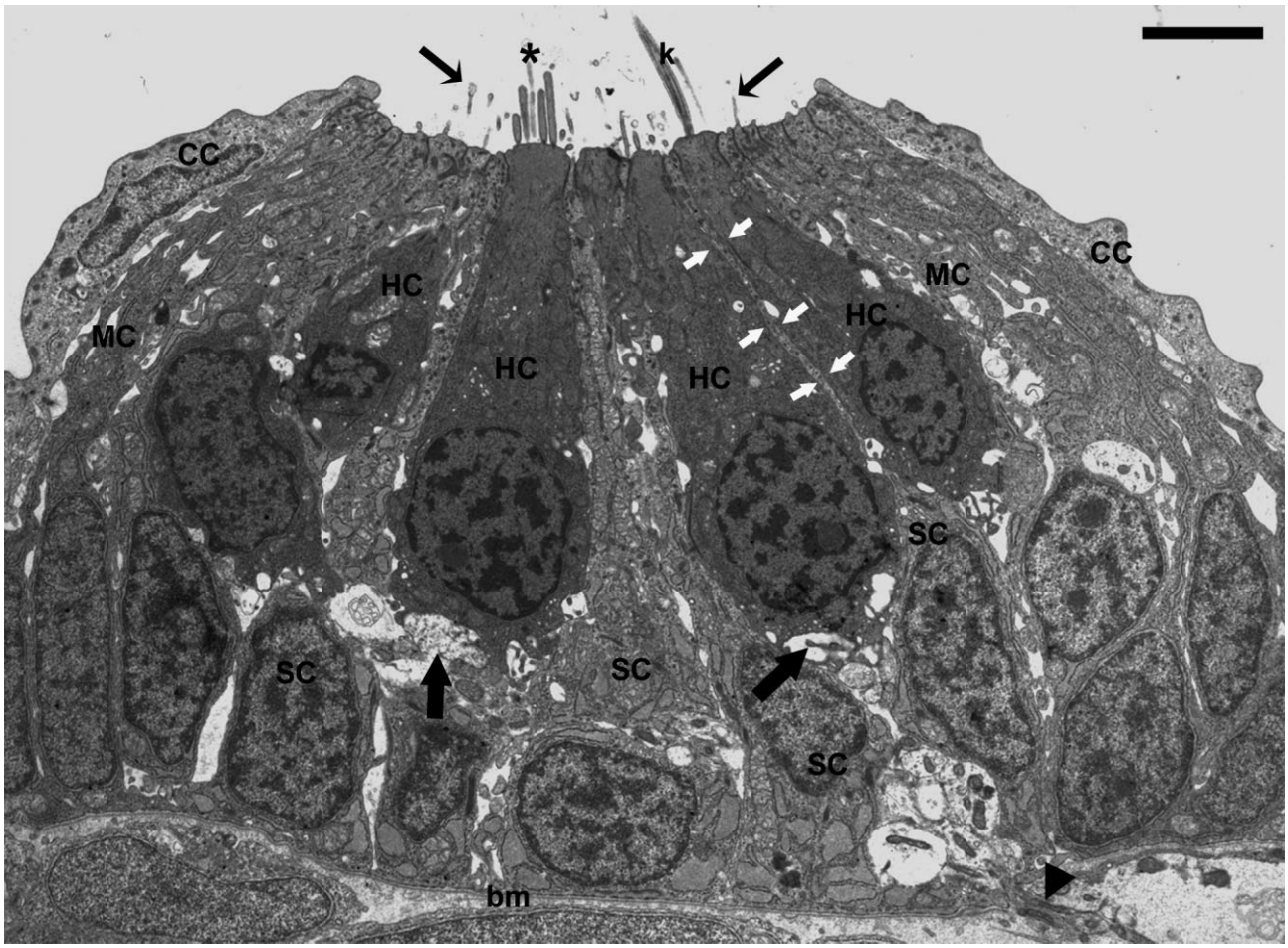

Fig. 2. Transmission electron micrograph of a transverse section through a neuromast of a zebrafish 5 dpf larva. Bottle-shaped hair cells (HC) are seen centrally. A stereocilia bundle (asterisk) from one of the hair cells and a kinocilium (k) from another are present, projecting from the apical surface of the hair cells. Underlying the hair cells are support cells (SC) with lighter cytoplasm and processes separating HCs, which extend to the apical surface (between white arrows) where they bear microvilli (thin black arrows). The HCs and SCs are enclosed by mantle cells (MC) and crescent cells (CC). A basement membrane (bm) underlies the neuromast below the support cell layer. Nerve fibers (black arrowhead) are seen crossing the basilar membrane and ending at the base of HCs (large black arrows). Scale bar = 3 μm.

induced alterations. To establish the baseline characteristics of the lateral line HCs we assessed in detail mock-treated wildtype zebrafish larvae at 5 dpf (control animals with all transfers performed as in neomycin-exposed fish but in embryo medium). The neuromasts are structures composed of HCs and support cells, which project volcano-like from the surface of the larval zebrafish. The stereotypical location of the neuromasts of the anterior lateral line, surrounding the head, and the posterior lateral line, along the midline of the tail, are illustrated schematically in Figure 1A. Each neuromast contains 3–15 HCs at this age (Harris, et al., 2003; Santos et al., 2006). Preferential labeling of HCs by vital dyes such as DASPEI (a mitochondrial dye) and YO-PRO-1 (a DNA dye) reveals their organization in grape-like rosettes (Fig. 1B–D). The overall ultrastructure of the neuromast is seen in transverse sections, as shown in Figure 2. The bottle-shaped HCs of one rosette are observed centrally and are encircled peripherally by mantle cells (MC) and overlying crescent cells (CC). The crescent cells are epithelial cells that overlie the outside of the neuromast, except at its center, where the apical surface of the HC and the support cells create a contiguous surface exposed to the outside of the animal. The support cell nuclei and the bulk of their cytoplasm (SC) are found in the layer below the HCs. However, cytoplasmic projections of the support cells extend to the apical surface and separate adjacent HCs (highlighted in one case by white arrows in Fig. 2). The proximal side of the neuromast is bound by a basement membrane (bm, Fig. 2). The afferent and efferent nerve fibers enter the neuromast basally through the basement membrane and contact the basal ends of the HCs.

HCs exhibit a dense granular cytoplasm with abundant mitochondria, ribosomes, and vacuoles (Fig. 2), in contrast to the more lightly stained, less dense cytoplasm of surrounding support cells. However, the density of the HC cytoplasm varies and, although less common at this stage, there are HCs with lighter cytoplasm (e.g., Fig. 3A, hc). Prominent nuclei with dense peripheral chromatin and heterogeneous interior regions are observed in both the

HCs and support cells. The nuclei of the HCs are located basally, with the bulk of the cytoplasm extending apically. There are stereocilia and a kinocilium present at the apical end of the HC, as seen in Figures 2 and 3A. Electron densities are seen at the base of the stereocilia where the actin filaments insert into the dense cuticular plate (noted by white arrows in Fig. 3B). Microvilli are present apically on support cells (black arrows in Figs. 2, 3A,B). Junctions between HCs and support cells are of two types: 1) zonula occludens junctions between HC cuticular plate and the apical part of support cells (arrowheads in Fig. 3C), and 2) desmosome-like junctions tightly attaching cells along the lateral walls to the base of HCs (arrows in Fig. 3C). Abundant mitochondria are found throughout the cytoplasm of the HCs (Figs. 2, 3A), including regions under the cuticular plate, along the lateral walls of the HC, and surrounding the nuclei both apically and basally (Fig. 3E). The mitochondria appear to have a tubular appearance, often extending a long distance longitudinally (e.g., Fig. 3D). Some mitochondria appear more discrete in size; however, it is not possible without serial sectioning to determine whether these are branches or ends of longer mitochondria or a population of smaller mitochondria. The HCs synapse basally with both afferent neurons and efferent endings (Fig. 3E). The presynaptic side of the afferent synapse typically contains a round synaptic body surrounded by synaptic vesicles, while the postsynaptic side is distinguished by an ending with clear cytoplasm and numerous mitochondria. Occasionally, these postsynaptic afferent endings appear swollen (Figs. 2, 3A), as in the initial steps of an excitotoxic process. The efferent synapse (Fig. 3E, labeled e) is characterized by a presynaptic ending filled with microvesicles and a postsynaptic cistern along the HC membrane.

Response to aminoglycosides is rapid

To observe the cellular events after aminoglycoside exposure, we examined the lateral line following brief exposure to neomycin over a range of concentrations (0–200 μM). We monitored the response in vivo by labeling HCs with the vital dye DASPEI. To observe the ultrastructural changes underlying this rapid HC response in vivo, we simultaneously prepared zebrafish larvae for TEM analysis in parallel to our in vivo examination. Larvae were exposed to neomycin for 15, 30, or 60 minutes, rinsed in fresh media, and either labeled with DASPEI and examined (Fig. 4) or immediately euthanized and fixed for TEM analysis (Figs. 6–10).

The in vivo response of larvae is illustrated in Figure 4 for four treatment conditions: 1) neomycin exposure for 60 minutes followed by a 180-minute recovery (in normal embryo medium); 2) neomycin exposure for 30 minutes and followed by a 60-minute recovery; 3) neomycin exposure for 30 minutes with no recovery period; or 4) neomycin exposure for 15 minutes and no recovery period. The first condition (60-minute exposure and 180-minute recovery) mirrors earlier results (Harris et al., 2003) and is provided for comparison with shorter exposures, which are the focus of this study. DASPEI is a mitochondrial potentiometric dye, and thus monitors loss of mitochondrial potential and/or loss of HCs. Examples of HCs stained with DASPEI are shown for the shorter time courses in Figure 4A–H. HCs show robust staining in mock-treated control (Fig. 4A,B). Larvae exposed to a low, 25-μM dose of neomycin exhibit little change in DASPEI staining from controls, as seen in Figure 4C (15 min exposure) or 4D (30 min exposure). Reduction in DASPEI staining is observed following short 15-minute (Fig. 4E) or 30-minute (Fig. 4F) exposures to 50 μM neomycin. Among larvae exposed to a high, 200-μM dose of neomycin (Fig. 4G,H), DASPEI staining is markedly reduced with increasing time from onset of drug exposure. Exposure to 200 μM neomycin for either 30 or 60 minutes with a recovery period results in a maximum loss of HC labeling by DASPEI that is not statistically different (Fig. 4). This loss is significantly attenuated with 15- or 30-minute drug exposure without a recovery period. Surprisingly, the response of HCs to the lower doses of neomycin is relatively constant regardless of time between drug exposure and examination (see 25- or 50-μM doses in Fig. 4).

Rapid changes in mitochondria occur in vivo following aminoglycoside exposure

DASPEI is reported to be a mitochondrial potentiometric dye. To verify and more precisely follow mitochondrial changes in vivo, we performed time-lapse imaging of early response to aminoglycosides (Fig. 5) using MTG to monitor mitochondrial mass and MTR to assess the presence of mitochondrial potential. We examined the response of mitochondria in HCs at 5-minute intervals for 30 minutes. HC mitochondria labeled with either dye alone exhibit little bleaching over the imaging period (MTG, Fig. 5A,B, or MTR, Fig. 5C,D) and little bleed-through between channels. HC mitochondria of mock-treated controls colabeled with MTR and MTG dyes show robust staining at the end of the 30-minute imaging window (Fig. 5E). By contrast, after treatment with 50 μM neomycin there is a dramatic loss of MTR fluorescence (Fig. 5F), indicative of a loss of mitochondrial potential with ongoing aminoglycoside exposure. To quantify this effect we determined the ratio of MTR to MTG fluorescent intensities within each neuromast (summed across optical sections) for each timepoint. The mean change in MTR/MTG ratio is plotted in Figure 5G for neuromasts of fish treated with no drug (mock-treated controls) or fish treated with 25 or 50 μM neomycin. There is a notable decrease in the MTR/MTG ratio over time, indicative of a loss of mitochondrial potential after neomycin exposure.

Ultrastructural changes in response to aminoglycosides

We sought to understand more precisely the types of subcellular events that lead to loss of HCs and therefore evaluated the ultrastructure of neuromasts under our treatment regimes. Quantitative results of the TEM analysis are shown in Table 1 and micrographs illustrating observations are shown in Figures 6–10.

To quantify the observations we made, we examined all of the neuromasts and HCs in our TEM grids and evaluated any alterations in each HC. We observed HCs with dilated mitochondria, condensed nuclei, fused stereocilia, dense cytoplasm, vacuolated light cytoplasm, and extrusion of HCs apically. The prevalence of these events is shown in Table 1. The most prevalent effect observed was mitochondrial swelling; mitochondria within HCs of animals exposed to neomycin are qualitatively less electron-dense, with fewer cristae present (Table 1, % HC mito damage; Fig. 9). We note that cristae have a consistent 20 nm size whether in control or neomycin-damaged mitochondria. We also enumerated those HCs with more se-

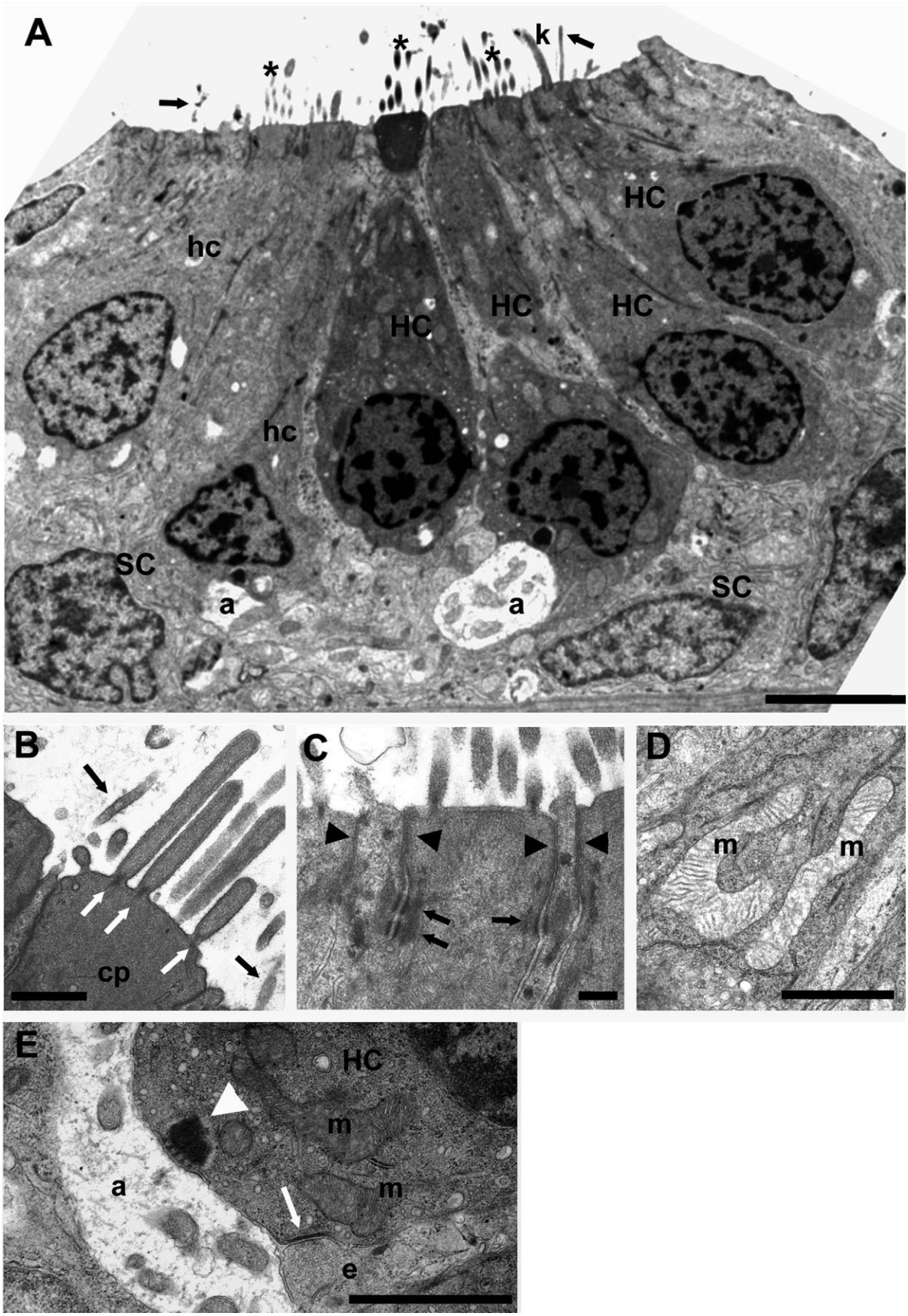

Figure 3

vere damage indicated by condensed or pyknotic nuclei or cytolytic hallmarks (Table 1, % of HC with severe damage). General conclusions drawn from the observations presented in Table 1 are that increasing time or dose corresponds to more prevalent mitochondrial changes and also to more HCs with severe damage. Increase in neomycin concentration had a more profound effect than increases in drug exposure time.

Figure 6 shows representative electron micrographs of neuromasts after exposure to a high (200 μM) dose of neomycin. This figure illustrates the effect of increasing neomycin exposure time on the response of HCs (Fig. 6A–C). In all cases there is marked damage among the HCs, and by 60 minutes of exposure most of the HCs have been removed from the epithelium.

Dying HCs in advanced stages of degeneration are observed even within 15 minutes of exposure to 200 μM neomycin, illustrating that neomycin-induced damage can occur rapidly (Fig. 6A). Collapse of the apical surface of neuromasts is typically evident. Severely damaged HCs can show an apoptotic-like appearance (asterisk in Fig. 6A) including swollen mitochondria, pyknotic or fragmented nuclei, and darkened cytoplasmic contents (indicated in Table 1 as % HC with condensed nuclei and % HC with dark cytoplasm). Alternatively, a more necrotic or cytolytic appearance (black arrowhead in Fig. 6A, and in Table 1 as % HC cytolytic) with swollen mitochondria, light cytoplasm and overall enlarged size is sometimes seen. Both types of damaged HCs can be observed in the same neuromast and can be in proximity, although cells with dark cytoplasm are more prevalent (see Table 1). Among HCs in these samples, 73% show some form of severe damage. At this high dose of neomycin most remaining HCs show some ultrastructural alteration, with 80% of HCs having mitochondrial alterations.

After 30 minutes of exposure to 200 μM neomycin and 1 hour recovery, most HCs observed show evidence of severe damage. Condensed, pyknotic nuclei are frequently observed (Fig. 6B). The same 30-minute drug exposure without any additional recovery time prior to fixation (Table 1) reveals that severely damaged cells can be observed already. We were not able to quantify the extent of damage in these treatment conditions since the severity of degeneration precluded accurate counting of HCs.

After 1 hour exposure to 200 μM neomycin, neuromasts show loss of almost all HCs (Fig. 6C). Clearing of the dead HCs has apparently occurred, as only sparse cell debris is seen. In contrast, support cells are found with a frequency comparable to wildtype and appear to have expanded their apical processes to fill the gaps. The location of some support cell nuclei is more apical than in neuromasts of untreated zebrafish. Edges of the epithelial cells are more closely apposed and correspond to an overall decrease and a flattening in the apical surface of the neuromast.

Aminoglycosides induce mitochondrial swelling in the zebrafish lateral line

In order to determine the first events in response to aminoglycosides in the zebrafish lateral line as detectable by TEM, we treated larvae with low doses of neomycin (50 and 25 μM) for short periods of time (15 or 30 minutes) and examined neuromast ultrastructure (Figs. 7, 8, respectively).

When zebrafish are exposed to 50 μM neomycin, the overall damage to HCs is less than that observed with 200 μM neomycin; 10–41% of HCs exhibit severe damage as compared to greater than 73% of HCs following exposure to 200 μM neomycin (Table 1). In addition, there is wide variability in the response to this lower dose. Figures 7A and 7B illustrate neuromasts representative of the extremes observed. Figure 7A shows a neuromast with severely damaged HCs following treatment with 50 μM neomycin for 15 minutes, including shrunken cells and condensed nuclei (Fig. 7A, asterisk and arrowheads, respectively). In this example the apical surface of the neuromast is deformed centrally, as if it has collapsed. However, unlike treatment with 200 μM neomycin, where this is a common feature, treatment with 50 μM neomycin usually leaves the overall structure of the neuromast largely intact. Some neuromasts show relatively little damage, such as that in Figure 7B, where HCs exhibiting no apparent damage reside alongside HCs with swollen mitochondria.

Overall, the most predominant cellular alteration observed after treatment with 50 μM neomycin was swollen mitochondria (37–67% of HCs, Table 1, Fig. 9). Mitochondria surrounding the nuclei appear more affected than those located more distantly within the HC. The swollen mitochondria often occupy a relatively large proportion of the cytoplasm as in Figures 7C,D or 10G. To a lesser extent, we observed other cellular damage, as tabulated in Table 1. Alterations observed include nuclear condensation (as in Fig. 7A, arrowheads), swollen cytolytic HCs (e.g., Fig. 7D, denoted by the black asterisk) or shrunken HCs with dark cytoplasm (e.g., Fig. 7D, denoted by the white asterisk), and fusion of stereocilia (e.g., Fig. 7A or 7D, white asterisks).

Following treatment with 25 μM neomycin for 15 minutes, most HCs are fairly normal in appearance. Figures 8A and 8B show neuromasts following exposure to 25 μM neomycin for 15 minutes to illustrate the range of damage observed. Some HC nuclei appear homogeneous without exhibiting shrinkage (see Fig. 8A, asterisk), suggesting that nuclear condensation is just beginning. While the majority of HCs show no apparent nuclear response, substantial numbers show a mitochondrial response (19–

Fig. 3. TEM micrographs of wildtype neuromast ultrastructure. **A:** Heterogeneity among hair cells within a neuromast can be observed. Some hair cells (HC) have dense, darkly stained cytoplasm while others (hc) have less dense cytoplasm. The even lighter cytoplasm of support cells (SC) can be observed between the hair cells. At the basal pole of two of the hair cells a synaptic body is seen facing a swollen afferent nerve ending (a). Kinocilium (k), microvilli (black arrows), and groups of stereocilia (asterisks) are observed apically. **B:** Higher magnification of the apical surface of a hair cell from Figure 2. Stereocilia are embedded in a cuticular plate (cp); the actin filaments and their rootlets (white arrows) are clearly seen. Note some microvilli (black arrows) on the top of adjacent support cells. **C:** Higher magnification of the apical surface of several hair cells and intervening support cells. Zonula occludens between HC and SC (black arrowheads) form a tight apical surface. Desmosomal-like junctions are present more basally (black arrows). **D:** Higher magnification of normal hair cell mitochondria (m) with regularly spaced cristae. **E:** Higher magnification of a hair cell (HC) synaptic pole. Both afferent (a) and efferent (e) endings are seen in this section as well as nearby mitochondria (m). The afferent ending has a clear cytoplasm and opposes a classical presynaptic body (white arrowhead) surrounded by a ring of microvesicles. The efferent ending is filled with microvesicles and faces a postsynaptic cistern (white arrow). Scale bars = 3 μm in A; 0.5 μm in B,D; 0.2 μm in C; 1 μm in E.

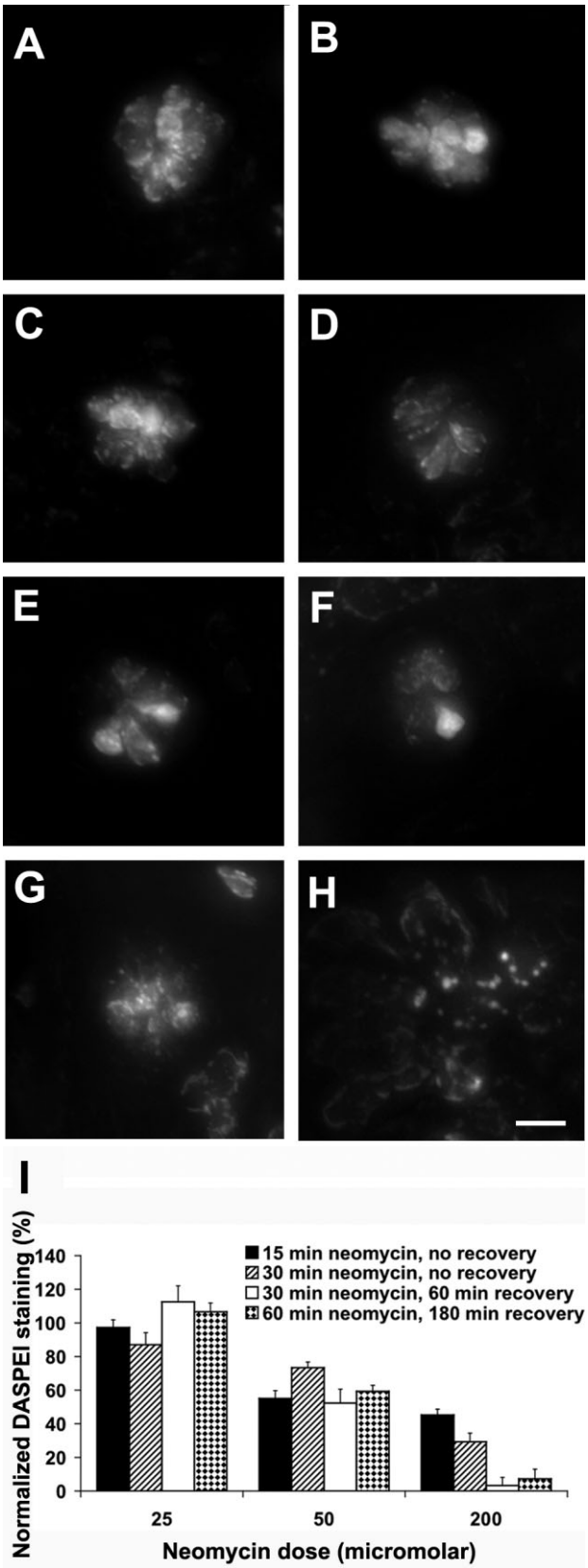

49%, Table 1). Rare HCs showed evulsion of the cuticular plate (Fig. 8D) or stereocilia fusion, in concert with mitochondrial swelling. In contrast, most HCs with mitochondrial responses had normal stereocilia and cuticular plate morphology.

Mitochondria from HCs and from adjacent afferent endings or support cells are shown in Figure 9 at higher resolution. In mock-treated control animals the mitochondria typically have tightly packed well-ordered cristae (Fig. 9A, hcm, and 9B), similar in appearance to those in nearby afferent mitochondria (Fig. 9A, am). In contrast, the mitochondria of HCs treated with neomycin often show swelling (Fig. 9E,I, hcm), although nearby afferent mitochondria resemble afferent mitochondria in untreated animals. At low doses of neomycin or short times, mitochondria with a relatively normal appearance can also be observed (Fig 9C, hcm, 9D,G, hcm). Swelling in the mitochondria appears as increased translucence in the mitochondrial matrix, while the leaflets of membrane forming the cristae often remain apposed (Figs. 10G,H, 6E,F). Examples of swollen HC mitochondria at high resolution are seen in Figure 9E,F,H–J. In animals treated with neomycin for 15 or 30 minutes the mitochondria of the afferent endings and support cells appear unaltered (Fig. 9A,C,E,G,I, am or scm, and 9K). Swelling of nerve endings is sometimes observed, consistent with an excitotoxic response (e.g., Sun et al., 2001; reviewed by Pujol and Puel, 1999), but even in these cases the mitochondria within the endings show normal morphology.

There is variability in the extent to which mitochondria within HCs respond to drug treatment (Fig. 10). In some

Fig. 4. In vivo response of hair cells to neomycin exposure as monitored by DASPEI staining. **A–H:** Brightest point projections of the IO2 hair cell labeled with DASPEI from mock-treated or neomycin-treated larvae. Larvae were treated for 15 minutes (A,C,E,G) or 30 minutes (B,D,F,H). A,B: mock-treated control fish. C,D: 25 μM neomycin, E,F: 50 μM neomycin. G,H: 200 μM neomycin. **I:** Graph of the percentage of DASPEI staining (normalized to that of untreated controls fish) observed with different treatment courses. Larvae were treated with 25, 50, or 200 μM neomycin (10, 75, 110 μM doses not shown) for 15–60 minutes, rinsed in fresh embryo medium three times, and allowed to recover for 0–180 minutes before labeling with DASPEI. Four treatment regimes differing in the time following onset of drug exposure: 15-minute exposure with no recovery (filled bars), 30-minute exposure with no recovery (striped bars), 30-minute exposure and a 60-minute recovery (open bars), or 60-minute exposure and 180-minute recovery (hatched bars). Error bars indicate SEM. For each dose and treatment regime, 10 neuromasts on 6–15 fish (60–150 neuromasts) were evaluated. By two-factor ANOVA, there is a significant effect of neomycin dose ($P < 0.001$) when considered as a single variable. Reduced hair cell staining was observed with increasing dose of neomycin (compare all treatments at 25 μM neomycin to all treatments at 50 μM neomycin to all treatments at 200 μM neomycin). No statistically significant effect of different treatment protocols alone was observed ($P > 0.01$). However, there is a significant interaction of treatment and dose ($P < 0.001$). At lower doses (25 and 50 μM neomycin), the degree of hair cell staining is similar with all treatments (compare bars for treatments with 25 μM neomycin to each other or compare bars for treatments with 50 μM to each other). In contrast, with a dose of 200 μM neomycin the degree of DASPEI staining differs depending on the treatment. There is significantly less hair cell staining observed with 30 min exposure with no recovery as compared to 15 min exposure with no recovery, and significantly less hair cell staining with longer treatments (30 min exposure and 60 min recovery or 60 min exposure and 180 min recovery). Scale bar = 10 μm.

HCs all of the mitochondria exhibit swelling, as in Figure 10E. Other HCs contain swollen mitochondria near the nucleus and normal mitochondria more apically (Fig. 10C). Figure 10D illustrates an example of swelling varying along a single mitochondrion, in which the portion of the mitochondrion next to the nucleus is swollen but the remainder is not. HCs with mitochondrial swelling appear at times next to HCs without any apparent alteration (Figs. 8A, 10C,D). Although we have observed examples of nuclei with perinuclear clearing (e.g., in Fig. 10H), we also see examples of HCs with notable mitochondrial swelling in the absence of such perinuclear effects (Fig. 10E), suggesting that this visible nuclear reaction occurs subsequent to the mitochondrial response. Generally, the HCs that show minimal damage have less dense cytoplasm. Mitochondria of afferent neurons (e.g., Figs. 7D, 10E) and support cells (e.g., Fig. 10E) appear normal, even when maintaining synaptic contact with HCs that have swollen mitochondria. Similarly, normal-appearing presynaptic bodies were often observed on otherwise deranged HCs (Figs. 7D,E, 10H).

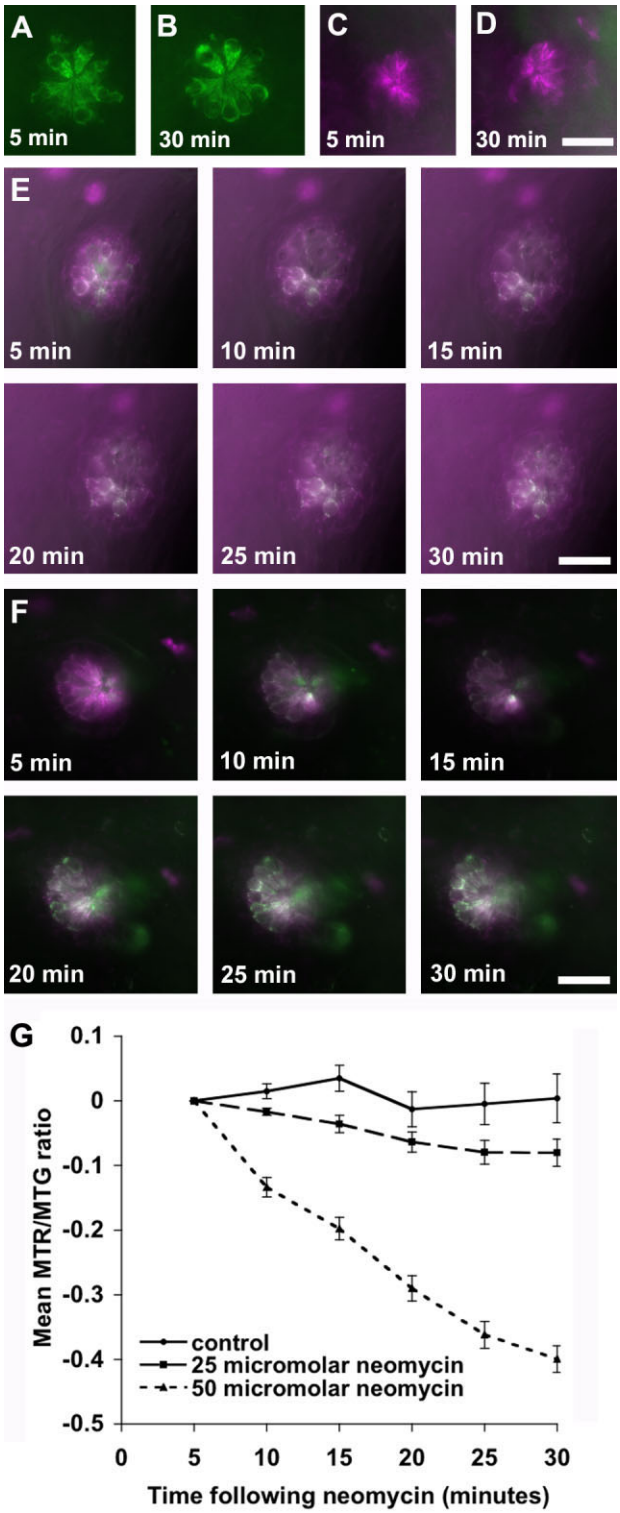

Fig. 5. Time-lapse imaging of the early response of hair cells to aminoglycosides. Hair cells are labeled with Mitotracker Red (MTR) to detect mitochondrial potential and with Mitotracker Green (MTG) to monitor mitochondrial mass. Constant exposure times were used at all timepoints. **A–F:** Raw images of a neuromast imaged with MTR and/or MTG. Each image is a representative optical slice taken from a z-stack encompassing the neuromast and cropped with no additional image processing. A,B: Neuromast of a mock-treated control fish labeled with MTG only at 5 minutes (A) and 30 minutes (B). C,D: Neuromast of a mock-treated control fish labeled with MTR only at 5 minutes (C) and 30 minutes (D). E: Images of the SO2 neuromast of a mock-treated control fish colabeled with both MTR (magenta) and MTG (green) are shown. The white color indicative of overlapping MTR or MTG is retained after 30 minutes of imaging. The optical slices shown are selected from the z-stack at the same level of the neuromast. Note the optical slice at the 5-minute timepoint at the comparable level in the neuromast is one slice (1 μM) above those at other time points due to drift of the animal. F: Images of the SO2 neuromast of a fish treated with 50 μM neomycin. White-gray color indicative of overlap of Mitotracker Red and Green signals is visible at the 5-minute timepoint and is successively reduced in subsequent timepoints. The optical slices shown are selected from the z-stack at the same level of the neuromast. Note the optical slice at the 5- and 30-minute timepoints at the comparable level in the neuromast are at different locations in the z-stack due to drift of the animal. **G:** The ratio of mean summed fluorescence intensities from MTR and MTG across the z-stack are shown for neuromasts of mock-treated fish (solid line, n = 4), fish treated with 25 μM neomycin (dashed line, n = 7) or fish treated with 50 μM neomycin (dotted line, n = 7). Decline in the ratio of the potentiometric indicator MTR to the mitochondrial mass indicator MTG is observed with increasing time in 25 μM or 50 μM neomycin but not with mock-treated controls. Scale bars = 20 μm.

DISCUSSION

The goal of this study was to evaluate the initial structural and ultrastructural events in aminoglycoside-induced mechanosensory cell death in zebrafish lateral line hair cells. We have demonstrated that aminoglycoside response occurs remarkably rapidly in this system and we have begun to evaluate these early cellular events in vivo. Mitochondrial alterations are the predominant early structural alterations we observe.

Hair cells of the 5 day old zebrafish larva demonstrate features of maturity

The ultrastructural features of wildtype untreated neuromasts we report here parallel prior observations of the lateral line in zebrafish (Metcalfe, 1985; Williams and Holder, 2000) and in other species (Stone, 1933; Wersaell

TABLE 1. Percentage of Hair Cells with Different Types of Neomycin-Induced Damage

Neomycin (μM)	Drug Exposure (min)	Recovery Time (min)	n Fish	n NMs	n HCs[1]	% HC Mito Damage[2]	% HC Severe Damage[3]	% HC Dark Cyto[4]	% HC Cytolytic[5]	% HC Condensed Nuclei[6]	% HC Fused Cilia[7]	% HC Extrusion[8]
Control			**11**	**21**	**96**	**5**	**0**	**0**	**0**	**0**	**0**	**0**
25	15	0	4	9	47	19	2	2	0	0	2	0
25	15	15	2	3	13	38	0	0	0	0	0	0
25	30	0	7	15	92	49	4	2	3	2	3	1
25, all treatments	**all**	**all**	**13**	**27**	**152**	**38**	**4.6**	**2**	**2**	**1**	**3**	**1**
50	15	0	2	4	27	37	15	7	0	7	4	4
50	15	15	3	5	21	50	10	0	0	9	5	0
50	30	0	5	13	70	67	41	19	6	23	1	4
50, all treatments	**All**	**All**	**10**	**22**	**118**	**56**	**29.6**	**13**	**3**	**17**	**3**	**3**
200	15	0	4	6	45	80	73	15	13	42	0	4
200	15	15	2	2	12[9]	n.a.	100[9]	n.a	n.a.	n.a.	n.a.	n.a.
200	30	0	3	5	22[9]	n.a.	86[9]	n.a	n.a.	n.a.	n.a.	n.a.
200	30	60	1	3	17[9]	n.a.	82[9]	n.a	n.a.	n.a.	n.a.	n.a.
200	60	0	2	4	16[9]	n.a.	82[9]	n.a	n.a.	n.a.	n.a.	n.a.
200 all treatments			**20**	**20**	**113[9]**	**80[10]**	**81.4[9]**	**n.a**	**n.a.**	**n.a.**	**n.a.**	**n.a.**

NM, neuromasts; HC, hair cells; n.a., not applicable.
[1]Number (n) of hair cell (HCs) cannot be directly compared to number of neuromasts (NMs) as some neuromasts have been assessed at two planes of section; this accounts for n HCs / NM >5 (up to 10).
[2]The percentage of hair cells with mitochondrial damage as indicated by swollen mitochodria with less internal electron density.
[3]Severe damage is noted if hair cells show any of the following characteristics: condensed cytoplasm and nucleus, cytolytic or necrotic appearance, and/or extrusion.
[4]The percentage of hair cells with dark cytoplasm: hair cells with cytoplasm notably denser than observed in wildtype.
[5]The percentage of hair cells with cytolytic appearance observed as light cytoplasm as compared to controls with enlarged hair cells and often the presence of large vacuoles.
[6]The percentage of hair cells with condensed nuclei observed as dark homogeneous nuclear material.
[7]The percentage of fused cilia is calculated from the incidence among all scored hair cells. While not all hair cells have visible stereocilia, the majority do. Therefore, this percentage may be as much as a twofold underrepresentation of occurrence of stereocilia fusion.
[8]The percentage of hair cells in the process of extrusion, observed by blebbing of the cytoplasm beyond the apical surface of the neuromast.
[9]At 200 μM neomycin it is difficult to accurately count HCs which appear mainly as remnants and debris. Due to the severity of damage, mitochondrial damage cannot be scored.
[10]Determined only from 200 μM neomycin exposure for 15 minutes, where 36 HCs out of 45 (all well recognizable) had mitochondrial damage.

and Flock, 1965; Jorgensen and Flock, 1973; Fay and Popper, 1999). By 5 dpf these neuromasts have the hallmarks of maturity, including the presence of stereocilia with rootlets, intact synapses, and numerous mitochondria and dense cytoplasm indicative of metabolic activity. We note that kinocilia are associated with stereocilia bundles in adult lateral line HCs and are therefore not a sign of immaturity. Neuromasts of the anterior lateral line examined in this study develop between 34 and 72 hours postfertilization (Raible and Kruse, 2000). By 3.5 dpf, HCs of the zebrafish lateral line can respond to mechanical stimuli, as demonstrated by field potential recordings (Nicolson et al., 1998; Sidi et al., 2003). Onset of aminoglycoside sensitivity occurs by 4 dpf and appears to stabilize by 5 dpf (Murakami et al., 2003). Thus, our structural observations are consistent with other measures of maturity. Elaboration of the bony structures surrounding a subset of the neuromasts occurs after the first month of growth (Webb and Shirey, 2003). However, it is not known whether the sensory cells undergo any further structural development. In another teleost, *Astronotus ocellatus*, superficial neuromasts are reported to be more resistant to gentamicin than canal neuromasts (Song et al., 1995). It is unknown whether this distinction arises later in zebrafish development. In 5 dpf larval zebrafish all neuromasts respond similarly to aminoglycosides (this study and Harris et al., 2003).

Response of the zebrafish lateral line to aminoglycosides is rapid

Degeneration of HCs in the zebrafish lateral line occurred remarkably quickly, within 15 minutes of drug administration. This is consistent with the effects of neomycin and streptomycin in the lateral line of the fish *Apolchelius lineatus*, assayed by behavioral responses (Kaus, 1987). By contrast, aminoglycoside damage of sensory epithelium has been reported to be slower in vivo and in vitro in some other preparations, including mammals, avians, and bullfrog (Baird et al., 1993; Bhave et al., 1995; Lopez et al., 1997; Hirose et al., 2004; Wagner et al., 2005). There are several possible explanations for these differences.

First, the response time between species may reflect differences in administration of drugs. Systemic routes of administration require drug transit time to reach the target tissue and introduce the possibility of confounding drug metabolism prior to reaching the HC. Several studies have shown that the onset of damage is more rapid with acute injection protocols or intratympanic injections or pledgets than chronic systemic injections of aminoglycosides (Janas et al., 1994; Aran et al., 1999; Heydt et al., 2004). Our zebrafish are treated in vivo by direct immersion in the drug solution. Due to the external location of

Fig. 6. TEM micrographs of neuromast ultrastructure after exposure to 200 μM neomycin. **A:** Neuromast after 15-minute neomycin exposure with no recovery. This section of a highly damaged neuromast shows hair cells with two pyknotic nuclei (white asterisks) or a condensing nucleus (black asterisk) together with some other types of less frequent hair cell damage, such as a cytolytic cell (black arrowhead) and partly evulsed hair cells (black arrows). **B:** Neuromast after 30-minute neomycin exposure and a 60-minute recovery period. Several highly condensed fragmented nuclei (black arrows) are present. Two intact hair cells are visible: one with swollen mitochondria (black asterisk) and one with a normal appearance (HC). **C:** Neuromast after 60-minute neomycin exposure and no recovery period. In this section hair cells are absent and support cells (SC) fill the neuromast. Cellular debris of dead hair cell(s) (black asterisk) and remaining nerve endings (black arrows) are present. Scale bars = 5 μM.

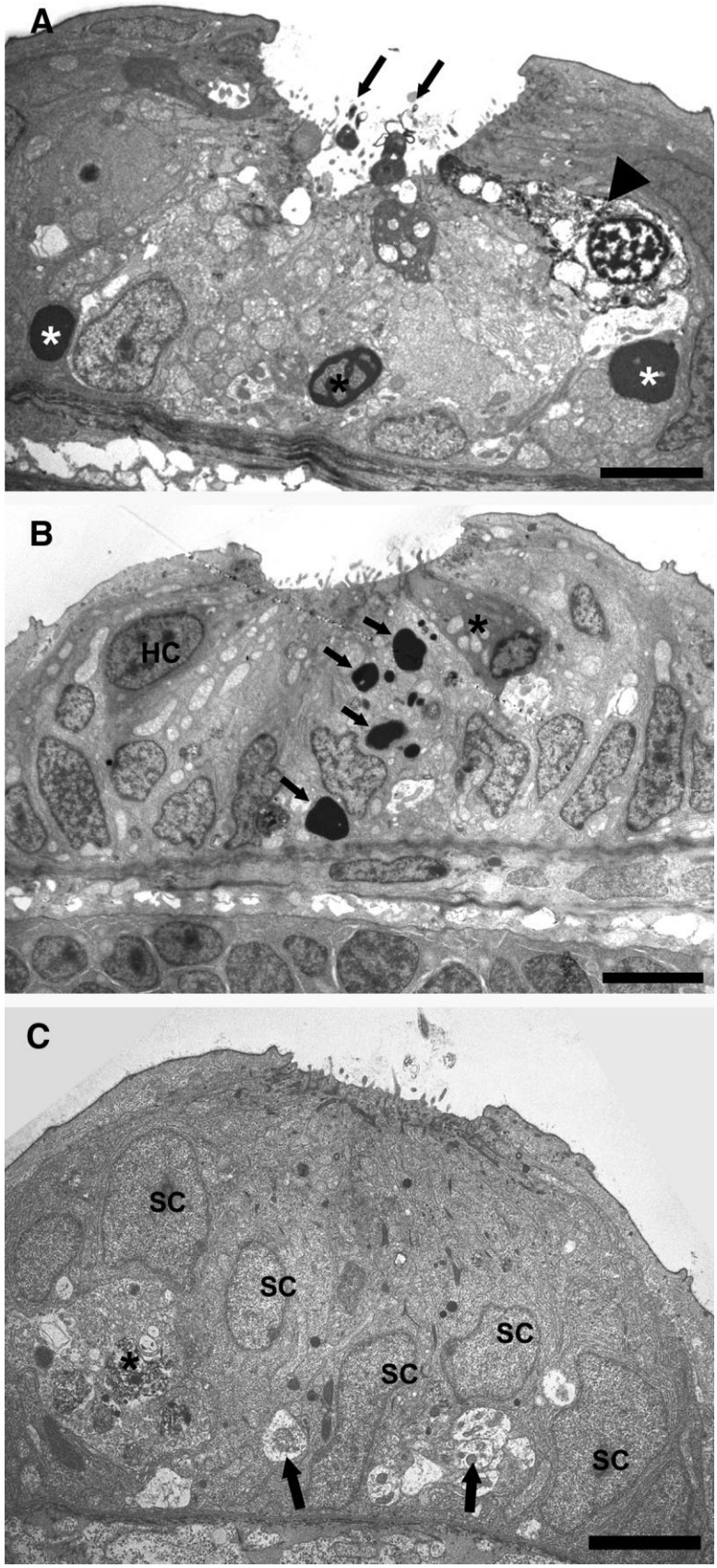

Figure 6

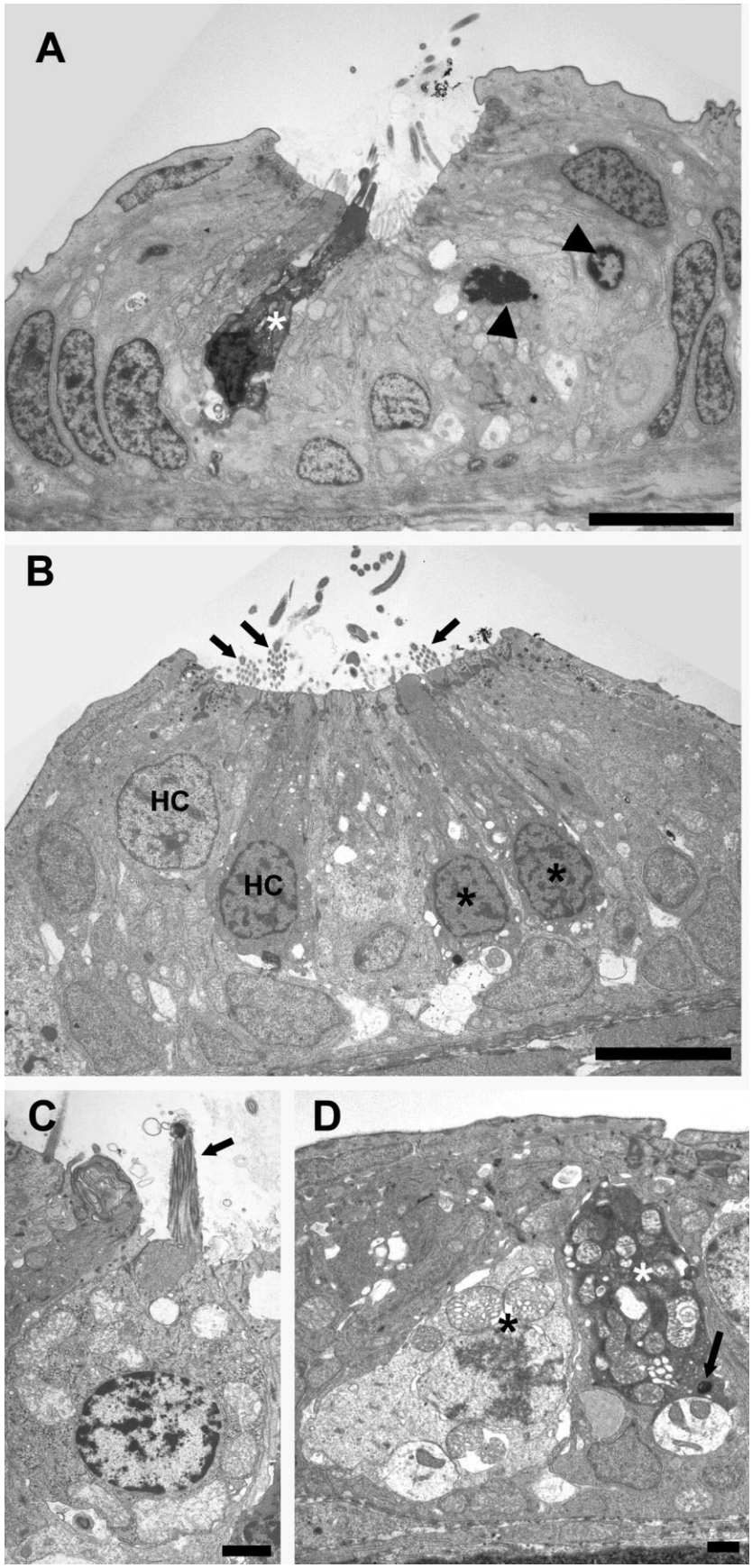

Figure 7

the HCs in the lateral line, confounding effects of systemic transit and dilution/metabolism of the drug are eliminated. On the other hand, systemic administration does not necessarily prolong drug accessibility. Gentamicin uptake and intracellular localization occurs within 30 minutes of direct exposure of bullfrog explants (Steyger et al., 2003), which is similar to the initial localization time seen when bullfrogs were systemically injected with gentamicin (Dai et al., 2006).

Second, differences in response times between species and tissues may reflect tissue-specific differences between the lateral line and the inner ear. There is experimental precedent for tissue-specific differences in aminoglycoside response (Cotanche, 1994; Forge and Schacht, 2000). Outer HCs in the cochlea are more sensitive than inner HCs, basal HCs more sensitive than apical, and vestibular type I HCs are generally more sensitive than type II HCs. Morphologically, zebrafish lateral line HCs are more vestibular-like in that they bear a kinocilium and, like type II vestibular HCs, have afferent innervation with bouton rather than calyx synapses. Some aminoglycosides are more vestibulotoxic than cochleotoxic, while the opposite is true of other aminoglycosides. Neomycin, used here, is reported to be more cochleotoxic than vestibulotoxic in some species (Hawkins and Lurie, 1953).

Third, differences in response time may reflect purely species-specific differences in uptake of aminoglycosides or activation of different response pathways. Direct comparison of the uptake time of fluorescently tagged gentamicin following systemic injection by Dai et al. (2006) revealed differences in the time of initial HC labeling postinjection between several vertebrates (30 minutes in bullfrog, 6 hours in chick, 3 hours in guinea pig, and 3–72 hours in mice). Furthermore, although aminoglycosides can reach the HCs in guinea pigs in 3 hours, the response of HCs typically is not observed until 6–24 hours (Tachibana et al., 1986; Hiel et al., 1993; Ding and Salvi, 2003; Imamura and Adams, 2003). On the other hand, some initial events have been reported to occur quite rapidly in vitro (where there is presumably less transit time required for drug to reach the HCs). In vitro cultures of sensory epithelium respond to aminoglycosides within a day (e.g., Matsui et al., 2000). Initial cellular responses can be rapid, e.g., reactive oxygen species (ROS) production occurred within 50–150 seconds of exposure to gentamicin in cultured chick basilar papillae (Hirose et al., 1999). Similarly, alteration in stereocilia stiffness induced by aminoglycosides occurs within 10 minutes of treatment (Kossl et al., 1990).

Notably, many of the intracellular events we observe in these zebrafish lateral line HCs are similar to early stages of damage observed in other species, despite differences in the time of response, suggesting that the processes are similar (Wersall and Hawkins, 1962; Ylikoski, 1974; Hirose et al., 1999, 2004). These observations, of course, do not rule out differences in the underlying signaling cascades. Only more thorough understanding of the necessary and sufficient cellular events as well as the alternative signaling cascades that can be accessed in each system will allow us to address this issue in an adequate way. This point has been emphasized by the findings of Schacht and colleagues (Jiang et al., 2006).

We observed that clearing of damaged HCs also can occur rapidly. By 60 minutes post-treatment, some neuromasts lack HCs while retaining an otherwise normal appearance. Rapid wound healing responses have been observed in many species of fish including zebrafish (Poss et al., 2003; Redd et al., 2004). It is perhaps not surprising that an aquatic animal would rapidly repair external damage. The majority of HC evulsion events occurred within 30 minutes of initial exposure to neomycin. This is consistent with reports that apoptotic cells are cleared within 1–2 hours (Weil et al., 1996). Movement of support cell nuclei apically is reminiscent of lumenal movements observed with regenerating HCs in chick (Duckert and Rubel, 1990; Hirose, et al., 2004). The evulsed cells were contiguous with adjacent support cells, indicating that junctions at the apical surface are maintained. This suggests that evulsion is a regulated process akin to that reported in other sensory epithelia (McDowell et al., 1989; Kelley et al., 1995; Leonova and Raphael, 1997). Some highly degenerate cells are also observed within the neuromast. It is not clear whether these are yet to be evulsed or whether they may be degraded or phagocytosed in situ as has been seen in some sensory epithelia (Forge, 1985; Fredelius and Rask-Andersen, 1990; Raphael et al., 1993; Jones and Corwin, 1996; Bhave et al., 1998).

Mitochondrial changes are an early response to aminoglycosides

The earliest and most prevalent alteration we observe at the ultrastructural level is mitochondrial swelling. With increasing exposure, dose, and/or survival time more HCs exhibit mitochondrial swelling. There is precedent for mitochondrial involvement in the aminoglycoside response of HCs. Early ultrastructure reports of chronic aminoglycoside exposure noted mitochondrial alterations including swelling alongside numerous other cellular changes (Friedman and Bird, 1961; Duvall and Wersall, 1964; Fermin and Igarashi, 1983; Lee et al., 1994). Notably, Bagger-Sjobak and Wersall (1978) observed progressively more severe mitochondrial swelling in the lizard lateral line after 7 and 21 days of chronic gentamicin treatment. However, it was not clear whether substantial HC loss had already occurred prior to their observations of these surviving HCs. The initial mitochondrial alterations they observed are reminiscent of the swollen mitochondria in the present study. There is also precedence for altered mitochondrial function in aminoglycoside-treated HCs.

Fig. 7. TEM micrographs of neuromast ultrastructure after exposure to 50 μM neomycin. **A:** Neuromast after 30-minute exposure and no recovery. Note the severe damage shown in this neuromast with its deformed apical surface. On the right, most hair cells have already degenerated, as seen by remnants of condensed cytoplasm and pyknotic nuclei (arrowheads). On the left, a hair cell (white asterisk) shows dark cytoplasm and nuclear condensation. Swollen mitochondria are also present. **B:** Neuromast after 15-minute exposure and no recovery. Most hair cells (HC) have a normal appearance, but some (black asterisks) have swollen mitochondria. Normal stereocilia bundles are observed on several hair cells (black arrows). **C:** Less commonly, hair cells exhibit fused stereocilia (arrow) in addition to swollen mitochondria. **D:** Higher magnification of two degenerating hair cells, both having swollen mitochondria. The left hair cell (black asterisk) with a clear cytoplasm seems to be starting a cytolytic process, while the right hair cell (white asterisk) with a dark and condensed cytoplasm appears to be undergoing an apoptotic-like process. Note that a presynaptic body (arrow) is still recognizable and mitochondria in the afferent ending are not swollen. Scale bars = 5 μm in A,B; 1 μm in C,D.

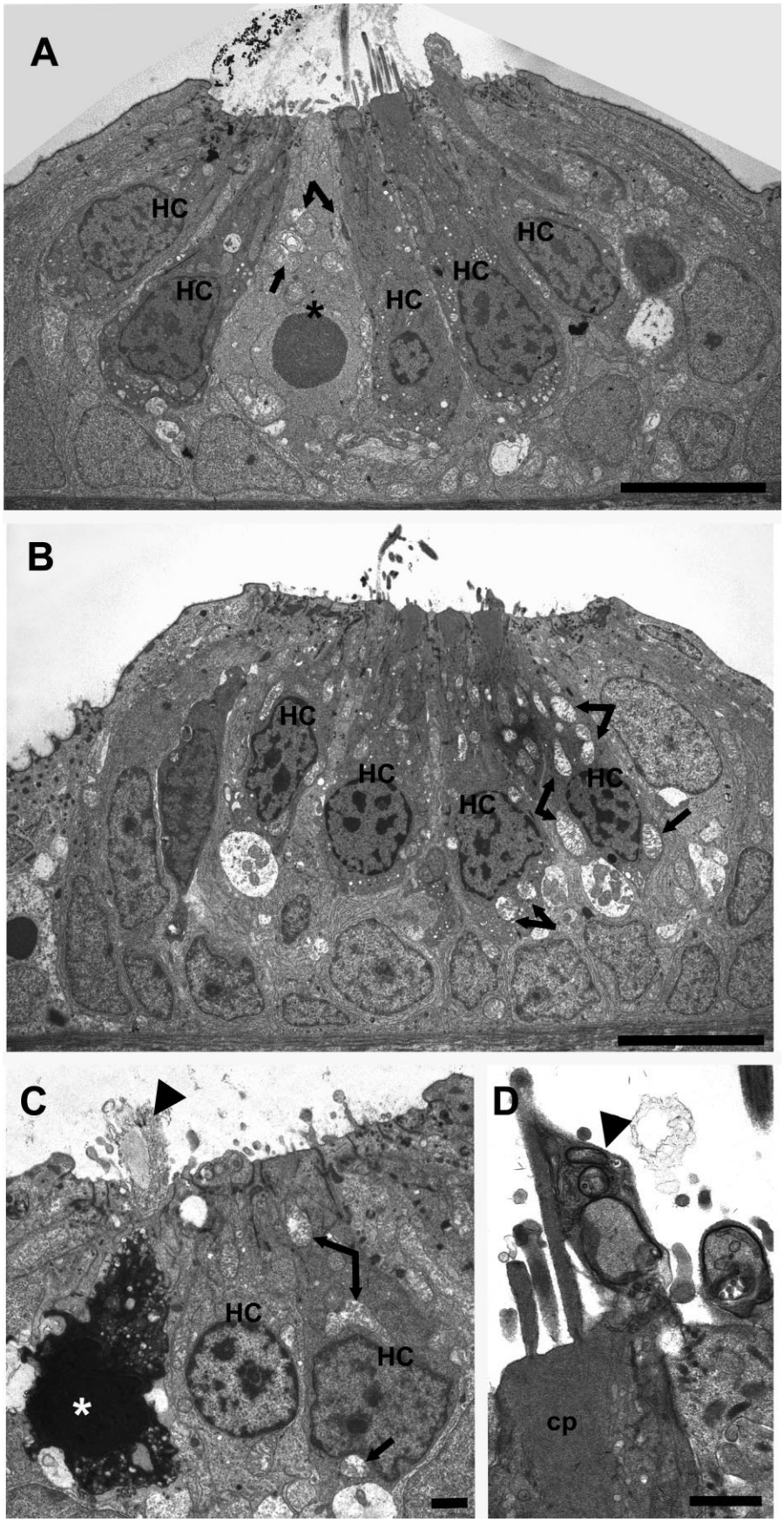

Figure 8

Hyde and Rubel (1995) observed that inhibition of mitochondrial protein synthesis increased gentamicin toxicity in chick auditory organ, suggesting that mitochondrial biogenesis plays a role in modulating HC damage. Aminoglycosides have been implicated in the production of ROS and the mitochondrion has been implicated as an organelle that functions in the intracellular regulation of ROS (Priuska and Schacht, 1995; Hirose et al., 1997; Sha et al., 1999; Wallace, 2005). Furthermore, mitochondrial dysfunction is thought to increase ROS levels and be implicated in noise- and age-related hearing loss (Henderson, 1999; Kopke, 1999; Nicotera et al., 2003; Pickles, 2003), and several antioxidants have provided some protection against acoustic as well as drug-produced damage (e.g., Schacht, 1999; Dehne et al., 2000; Wang et al., 2003; McFadden et al., 2003; Rybak and Whitworth, 2005). Perhaps the strongest indicator of a role of mitochondria in modulating HC damage is the existence of families bearing genetic mutations in mitochondrial genes (e.g., Fischel-Ghodsian, 1999; Guan et al., 2000; Pickles, 2003; Zhao et al., 2004).

We observed mitochondrial matrix expansion with retention of some cristae rather than swelling of the intermembrane space. Expansion of the mitochondrial matrix is classically associated with abnormal opening or transitioning of the mitochondrial transition pore (MTP), efflux of protons, and loss of mitochondrial membrane potential (Bernardi et al., 1994; Vander Heiden et al., 1997; Kroemer and Reed, 2000; Fernandez-Checa, 2003). Together, depolarization of the mitochondrial potential and expansion of the matrix is thought to lead to outer membrane rupture and subsequent release of intermembrane space apoptogenic proteins, such as cytochrome c, Smac/Diablo, AIF, and EndoG (Desagher and Martinou, 2000; Tsujimoto, 2003). Mather et al. (2001) demonstrated that aminoglycosides can induce rupture of outer mitochondrial membranes and release of soluble intermembrane proteins from liver mitochondria in vitro. Our in vivo assessment of mitochondrial membrane potential indicates that there is a rapid drop in mitochondrial membrane potential in the lateral line HCs prior to nuclear condensation or fragmentation. A similar loss of mitochondrial membrane potential was reported by Denhe et al. (2002) an hour prior to HC loss in the guinea pig cochlear explants during continual gentamicin exposure. Inhibition of the mitochondrial transition pore with cyclosporin A partially inhibited this depolarization. Analogously, Sandoval and Molitoris (2004) observed reduction in the mitochondrial membrane potential in kidney cells following gentamicin treatment and concluded that it may be one of the earliest effects on the proximal tubules cells.

Are mitochondria a direct or indirect target of aminoglycosides?

Two hypotheses for the role of mitochondria in aminoglycoside response are: 1) mitochondria are the direct target of aminoglycosides, or 2) mitochondria respond to other preceding cellular events within the cells. TEM analysis can only detect cellular events with a morphological correlate. Thus, while alteration of mitochondria is the first structural change we observe, it may not be the first cellular event. However, if cellular events occur prior to mitochondrial response they must occur rapidly (<15 minutes).

Several lines of evidence suggest that the mitochondrion may be a direct target of aminoglycosides. Aminoglycosides are localized to mitochondria in HCs, along with numerous other subcellular locations (Tachibana et al., 1986; Hiel et al., 1993; Ding and Salvi, 2003; Imamura and Adams, 2003; Steyger et al., 2003), making it plausible that they act at the mitochondrion. The bactericidal activity of aminoglycosides results from binding to the rRNA components of the small ribosome subunit and inhibition of translation (Davies, 1965). It has long been thought that aminoglycosides do not bind eukaryotic ribosomes due to their evolutionarily divergence (Wilhelm et al., 1978). Recent structural solutions of ribosome-bound aminoglycoside molecules indicated that the binding site is indeed divergent between the prokaryotic and eukaryotic ribosomal subunits (Recht et al., 1999; Vincens and Westof, 2003; Kaul et al., 2005). However, the mitochondrial ribosome resembles the prokaryotic ribosome (Gutell et al., 1994), suggesting that it may be a target of aminoglycosides. On the other hand, the rapidity of damage we observe would seem to preclude inhibition of protein synthesis at least for the most rapidly responding HCs. Yet recent identification of a yeast nuclear-encoded mitochondrial modifier capable of eliminating protein synthesis in the presence of a mutation conferring aminoglycoside susceptibility (Yan et al., 2005) supports the suggestion that mitochondrial translational apparatus can be a target of aminoglycosides. Other aspects of mitochondrial biology also could be targeted such as mitochondrial fusion/fission, which has recently been implicated in cell death responses (Chen and Chan, 2005).

Alternatively, the impact of aminoglycosides on mitochondria may be an indirect response to other cellular signals that coordinate cell death/survival responses (Danial and Korsmeyer, 2004). Studies from several groups indicate the activation of intrinsic, mitochondrially organized, cell death pathways in the response of HCs to aminoglycosides, although different initial triggering events have been noted. Studies by Mangiardi et al. (2004) and Myrdal et al. (2005) are consistent with a nuclear target for aminoglycosides, possibly via T-cell restricted intracellular antigen-related protein, TIAR. The efficacy of D-JNK-1, an inhibitor of the MAPK-JNK signaling pathways in prevention of HC loss, indicates a role of JNK during both drug- and noise-induced damage (Wang et al., 2003; Matsui et al., 2004). Ras activation also occurs with

Fig. 8. TEM micrographs of neuromast ultrastructure after exposure to 25 μM neomycin for 15 minutes and no recovery period (**A,B**) or 30 minutes and no recovery period (**C,D**). A: A neuromast exemplifying the most severe damage observed at 15-minute exposure to 25 μM neomycin. One hair cell (asterisk) has clear cytoplasm and an altered homogeneous nucleus with swollen mitochondria (arrows) among hair cells with a normal appearance (HC). A fragment of the extracellular cupula is visible above the neuromast. At the far right, a partially extruded hair cell is present. B: A neuromast exemplifying minimal damage. Most hair cells (HC) have a normal appearance, but some exhibit mitochondrial swelling (arrows). C: An example of the most severely damaged hair cell at 25 μM exposure for 30 minutes. This hair cell (white asterisk) exhibits a dense cytoplasm and nucleus, and evulsion of its cuticular plate (arrowhead). The adjacent two hair cells (HC) have a normal appearance, except for some mitochondrial swelling (arrows). D: A rare hair cell shows extrusion of cytoplasm (arrowhead) at the site of the kinocilium. Note the normal appearance of adjoining stereocilia and cuticular plate (cp). Scale bars = 5 μm in A,B; 1 μm in C; 0.5 μm in D.

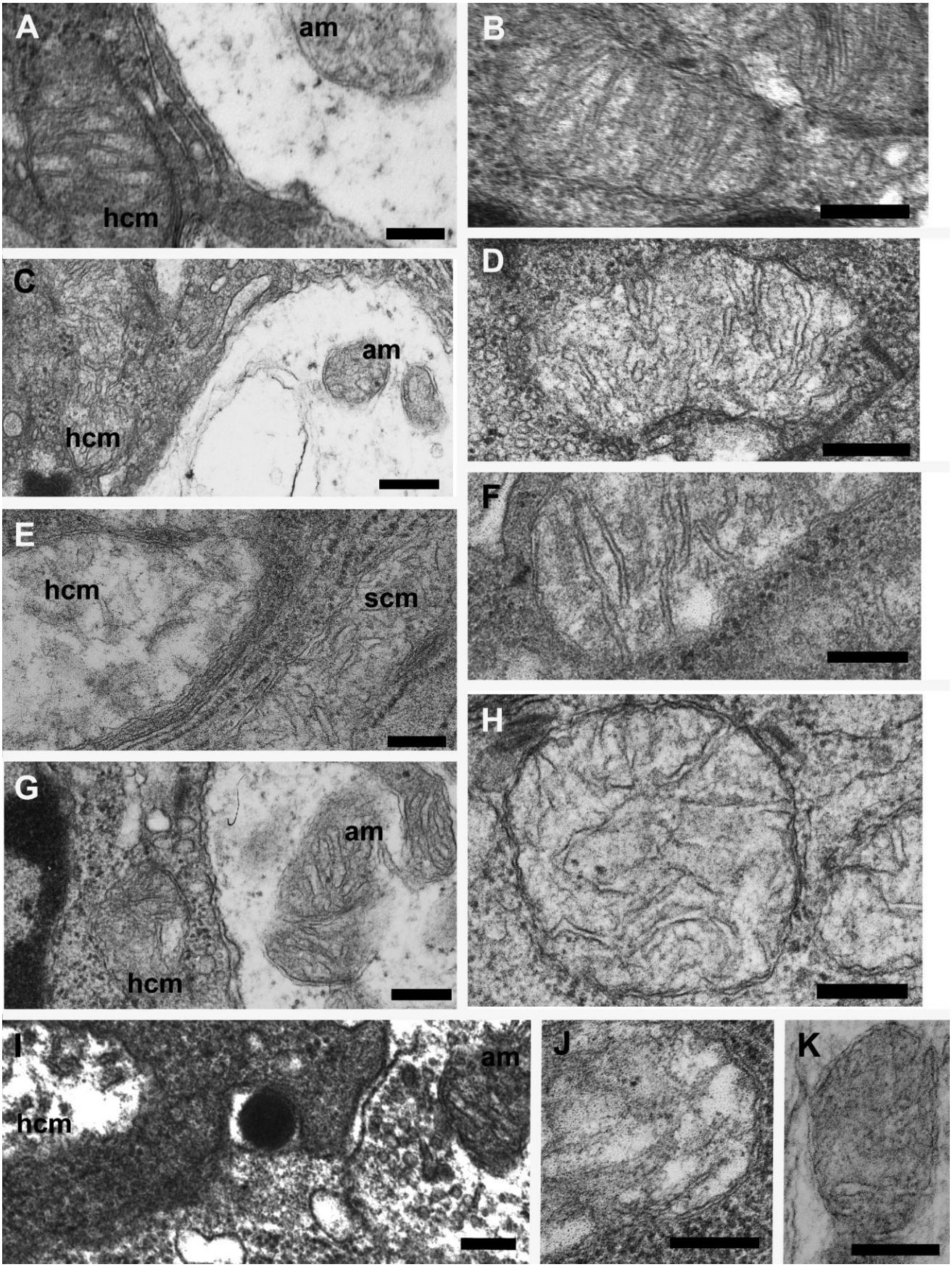

Fig. 9. TEM micrographs comparing mitochondria following neomycin treatment. **A,C,E,G,I:** Mitochondria in hair cell (hcm) next to mitochondrial in afferent ending (am in A,C,G,I) or support cell (scm in E). High-resolution images of mitochondria in hair cells (**B,D, F,H,K**) or afferent ending (**J**). A,B: Electron-dense mitochondria from mock-treated control fish. C,D: Treated with 25 μM neomycin for 15 minutes. E,F: Treated with 25 μM neomycin for 30 minutes. G,H: Treated with 50 μM neomycin for 15 minutes. I,J,K: Treated with 50 μM neomycin for 30 minutes. Scale bars = 200 nm.

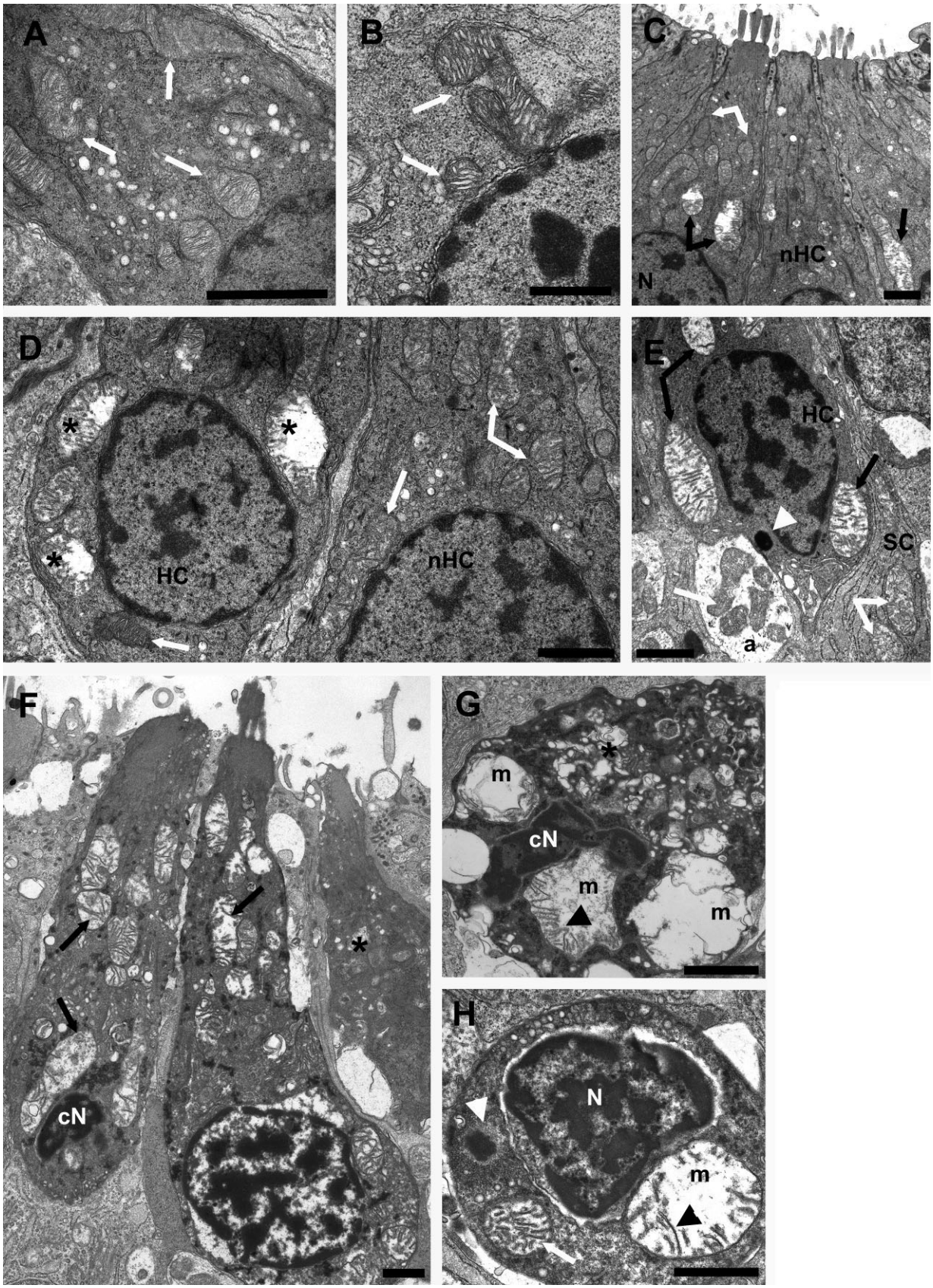

Figure 10

aminoglycoside exposure in vitro and may serve as the upstream activator of JNK (Battaglia et al., 2003). It remains to be determined which, if any, of these events precedes mitochondrial swelling and which are requisite for cell death in this system.

Heterogeneous cell death phenotypes

While mitochondrial swelling seems to be a central event that occurred in the majority of cells that are destined to degenerate, the events that occur after that are heterogeneous. Stereocilia fusion and HC evulsion (Furness and Hackney, 1986; Pickles et al., 1987; Takumida et al., 1989) were seen, but not particularly prevalent. A potential criticism is that, using TEM analysis, we may be underestimating the degree of stereocilia fusion. However, we do observe many HCs with normal stereocilia despite other intracellular alterations. Comparative analysis of HCs using SEM and TEM analyses indicated that cytoplasmic alterations appeared to precede stereocilia changes (Lenoir and Puel, 1987). Our observation of HC evulsion is consistent with apical protrusions and blebbing reported previously by many authors (e.g., Richardson and Russell, 1991; Forge and Richardson, 1993; Janas et al., 1995). Notably, although other studies have reported significant lysosomal inclusions (Ylikoski, 1974; Gratacap et al., 1985; Lenoir and Puel, 1987; Umemoto et al., 1994), we did not observe lysosomal inclusions. It is possible that degenerating HCs with severe damage might include these structures, perhaps reflecting a faster transition through these intermediate stages of damage. Alternatively, since most reports of abundant lysosomal inclusions have been in sensory epithelia treated with kanamycin, this may reflect a difference in the aminoglycoside used.

We observed occasional HCs with little ultrastructural change other than mitochondrial swelling even after high-dose neomycin treatment. This is consistent with retention of immature HCs following aminoglycoside exposure (Murakami et al., 2003; Santos et al., 2006). We also observed a few severely degenerated HCs in response to low-dose exposure. It is unclear why these particular HCs respond so dramatically. This may reflect a difference in the metabolic state of the HC at the time of drug exposure. Heterogeneity in resting mitochondrial ROS of brain astrocytes has been associated with variability in mitochondrial swelling and permeability transition after irradiation (Peng and Jou, 2004). Alternatively, such variability may reflect cell-to-cell variability in uptake of drug, as suggested by Imamura and Adams (2003) in guinea pig inner ear.

HCs with apoptotic-like features and those with necrotic-like features include massive organelle failure and seem unlikely to be reversible. However, many structural alterations may be survivable. For instance, Gale et al. (2002) observed HCs in bullfrog saccular cultures that had lost stereocilia bundles in response to low doses of aminoglycosides could survive and replace their bundles. At low aminoglycoside dose (25 μM), we observed that nearly half of the HCs had alterations in mitochondria, but few die, even at longer survival times.

Finally, and most prominently, we observed two quite distinct forms of degeneration, particularly with higher doses (50–200 μM). Previous studies have reported both apoptotic-like HC death and necrotic-like HC death in response to aminoglycosides (e.g., Darrouzet and Guilhaume, 1974; Park and Cohen, 1984; Nakagawa et al., 1997; Lopez et al., 1997; Vago et al., 1998; Lenoir et al., 1999; Forge and Li, 2000). Ultrastructural comparison of aminoglycoside-induced cell death and staurosporin-induced cell death of rodent vestibular explants demonstrated that the majority of HCs were lost by an apoptotic-like process within 24 hours following treatment with 1 mM gentamicin (Forge and Li, 2000). In contrast, Jiang et al. (2006) observed both necrotic and apoptotic-like HC death. Aminoglycosides can induce apoptotic-like, caspase-dependent cell death pathways including release of cytochrome c and activation of caspases 3 and 9 (Forge and Li, 2000; Cunningham et al., 2002; Cheng et al., 2003; Lee et al., 2004; Matsui et al., 2004). Inhibition of Jun kinase (Pirvola et al., 2000; Matsui et al., 2002; Ylikoski et al., 2002; Wang et al., 2003), inhibition of caspase 3, activation of caspase 9 (Cunningham et al., 2002; Cheng et al., 2003), or overexpression of anti-apoptotic Bcl2 (Cunningham et al., 2004) can attenuate aminoglycoside-induced HC death. In contrast, HC death following chronic exposure to aminoglycosides in rodents can also occur along caspase-independent pathways via EndoG release from the mitochondria and calpain activation (Ladrech et al., 2004; Jiang et al., 2006).

Our TEM observations indicate that necrotic-like HCs can occur in close proximity to apoptotic-like HCs within the same neuromasts. This argues that the manner of cell death is driven by cell-to-cell variability rather than species or end organ-specific limitations. Our time and dose

Fig. 10 (Overleaf). Variability among hair cells in the response of mitochondria induced by neomycin. **A:** Neuromast of a mock-treated control contain normal mitochondria (white arrows) with tightly packed cristae. **B:** Higher resolution of a control neuromast with normal mitochondria (white arrows). **C–E:** Neuromasts after 30-minute exposure to 25 μM neomycin. C: Different mitochondrial morphology between adjacent hair cells. Leftmost and rightmost hair cells exhibit swollen mitochondria (black arrows) near their nuclei (N) and normal mitochondrial more apically (white arrows). A neighboring hair cell has a normal appearance (nHC). D: Adjacent hair cells. Nuclei in both cells appear unaffected. The hair cell on the right (nHC) shows little or no response including mitochondria with a normal appearance (white arrows). In contrast, the hair cell (HC) on the left exhibits swollen mitochondria (black asterisks). Note the intraorganellar variation in swelling with disruption of the alignment of cristae in some regions of the mitochondria but not in other regions. A normal mitochondrion (white arrow) is also present. E: High magnification of the basal pole of a damaged hair cell (HC) with an intact synaptic body (white arrowhead). Note the multiple mitochondria with pronounced swelling (black arrows) around the hair cell nucleus, whereas the afferent ending (a) and the support cell (SC) both contain unswollen mitochondria (white arrows). **F,G:** Neuromasts following exposure to 50 μM neomycin. F: Adjacent hair cells, one with swollen mitochondria and pyknotic nuclei (cN) and its neighbor with a typically sized nucleus showing denser chromatin. Both hair cells have swollen mitochondria (examples shown by black arrows) throughout the cells. A more damaged cell with dense cytoplasm is also seen (black asterisk). G: Hair cell with severely degenerating cytoplasm (black asterisk) and multiple mitochondria with extreme swelling (m) and fragmenting condensed nucleus (cN). Note the retention of apposed membranes of some of the cristae (black arrowhead) despite the extreme swelling of the mitochondrion. **H:** The base of a rare surviving hair cell after 15-minute exposure to 200 μM neomycin. The nucleus (N) is surrounded by a reactive (light) zone. A swollen mitochondrion (m) with partially intact cristae (black arrowhead) is present, as well as a mitochondrion without appreciable swelling (white arrow). Note the normal presynaptic body (white arrowhead) surrounded by synaptic microvesicles. Scale bars = 1 μm in A,C–H; 0.5 μm in B.

data suggest that mitochondrial swelling precedes both forms of cell death. However, TEM data is, by its nature, a static snapshot of cellular conditions. Further studies will be required to sort out the actual pathways that are both necessary and sufficient for death or survival to occur. A growing body of evidence indicates that the mitochondrion coordinates and conveys signals for cell survival and cell death (Minamikowa, 1999; Newmeyer and Ferguson-Miller, 2003). We suggest that mitochondrial response may be an early, common checkpoint preceding multiple forms of cell death in sensory epithelia.

ACKNOWLEDGMENTS

The authors thank Lisa Cunningham, Felipe Santos, and Les Westrum for advice in the early stages of this project, and Jameel Itani, Steve McFarlane, and Stephanie Lara for technical assistance with ultrastructural preparations.

LITERATURE CITED

Adams JM. 2003. Ways of dying: multiple pathways to apoptosis. Genes Dev 17:2481–2495.

Akiyoshoi M, Yano S, Nakada H, Sato K, Shoji T. 1976. Study on damage of the vestibular organs due to aminoglycoside antibiotics by means of supravital reduction of nitro-BT. Ear Res Jpn 7:98–100.

Aran JM. 1995. Current perspectives on inner ear toxicity. Otolaryngol Head Neck Surg 112:133–144.

Bagger-Sjoback D, Wersall J. 1978. Gentamicin-induced mitochondrial damage in inner ear sensory cells of the lizard Calotes versicolor. Acta Otolaryngol 86:35–51.

Baird RA, Torres MA, Schuff NR. 1993. Hair cell regeneration in the bullfrog vestibular otolith organs following aminoglycoside toxicity. Hear Res 65:164–174.

Baird RA, Burton MD, Fashena DS, Naeger RA. 2000. Hair cell recovery in mitotically blocked cultures of the bullfrog saccule. Proc Natl Acad Sci U S A 97:11722–11729.

Battaglia A, Pak K, Brors D, Bodmer D, Frangos JA, Ryan AF. 2003. Involvement of ras activation in toxic hair cell damage of the mammalian cochlea. Neuroscience 122:1025–1035.

Bernardi P, Broekemeier KM, Pfeiffer DR. 1994. Recent progress on regulation of the mitochondrial permeability transition pore; a cyclosporin-sensitive pore in the inner mitochondrial membrane. J Bioenerg Biomembr 26:509–517.

Bhave SA, Oesterle EC, Coltrera MD. 1998. Macrophage and microglia-like cells in the avian inner ear. J Comp Neurol 398:241–256.

Chen H, Chan DC. 2005. Emerging functions of mammalian mitochondrial fusion and fission. Hum Mol Genet 14 Spec No. 2:R283–289.

Cheng AG, Cunningham LL, Rubel EW. 2003. Hair cell death in the avian basilar papilla: characterization of the in vitro model and caspase activation. J Assoc Res Otolaryngol 4:91–105.

Coombs S, Montgomery JC. 1999. The enigmatic lateral line system. In: Fay RR, Popper AN, editors. Comparative hearing. Fish and amphibians. New York: Springer.

Cotanche DA, Lee KH, Stone JS, Picard DA. 1994. Hair cell regeneration in the bird cochlea following noise damage or ototoxic drug damage. Anat Embryol (Berl) 189:1–18.

Cunningham LL, Cheng AG, Rubel EW. 2002. Caspase activation in hair cells of the mouse utricle exposed to neomycin. J Neurosci 22:8532–8540.

Cunningham LL, Matsui JI, Warchol ME, Rubel EW. 2004. Overexpression of Bcl-2 prevents neomycin-induced hair cell death and caspase-9 activation in the adult mouse utricle in vitro. J Neurobiol 60:89–100.

Dai CF, Mangiardi D, Cotanche DA, Steyger PS. 2006. Uptake of fluorescent gentamicin by vertebrate sensory cells in vivo. Hear Res 213:64–78.

Dambly-Chaudiere C, Sapede D, Soubiran F, Decorde K, Gompel N, Ghysen A. 2003. The lateral line of zebrafish: a model system for the analysis of morphogenesis and neural development in vertebrates. Biol Cell 95:579–587.

Danial NN, Korsmeyer SJ. 2004. Cell death: critical control points. Cell 116:205–219.

Darrouzet J, Guilhaume A. 1974. [Ototoxicity of kanamycin studied day by day. Experimental electron microscopic study]. Rev Laryngol Otol Rhinol (Bord) 95:601–621.

Davies J, Gorini L, Davis BD. 1965. Misreading of RNA codewords induced by aminoglycoside antibiotics. Mol Pharmacol 1:93–106.

Dehne N, Lautermann J, ten Cate WJ, Rauen U, de Groot H. 2000. In vitro effects of hydrogen peroxide on the cochlear neurosensory epithelium of the guinea pig. Hear Res 143:162–170.

Dehne N, Rauen U, de Groot H, Lautermann J. 2002. Involvement of the mitochondrial permeability transition in gentamicin ototoxicity. Hear Res 169:47–55.

Desagher S, Martinou JC. 2000. Mitochondria as the central control point of apoptosis. Trends Cell Biol 10:369–377.

Ding D, McFadden SL, Browne RW, Salvi RJ. 2003. Late dosing with ethacrynic acid can reduce gentamicin concentration in perilymph and protect cochlear hair cells. Hear Res 185:90–96.

Dijkgraaf S. 1963. The functioning and significance of the lateral line organs. Biol Rev 38:51–105.

Duckert LG, Rubel EW. 1990. Ultrastructural observations on regenerating hair cells in the chick basilar papilla. Hear Res 48:161–182.

Duvall AJ, Wersall J. 1964. Site of action of streptomycin upon inner ear sensory cells. Acta Otolaryngol 57:581–598.

Fermin CD, Igarashi M. 1983. Aminoglycoside ototoxicity in the chick (Gallus domesticus) inner ear: I. The effects of kanamycin and netilmicin on the basilar papilla. Am J Otolaryngol 4:174–183.

Fernandez-Checa JC. 2003. Redox regulation and signaling lipids in mitochondrial apoptosis. Biochem Biophys Res Commun 304:471–479.

Fischel-Ghodsian N. 1999. Genetic factors in aminoglycoside toxicity. Ann N Y Acad Sci 884:99–109.

Flock A, Flock B, Fridberger A, Jager W. 1997. Methods for integrating fluorimetry in the study of hearing organ structure and function. Hear Res 106:29–38.

Forge A. 1985. Outer hair cell loss and supporting cell expansion following chronic gentamicin treatment. Hear Res 19:171–182.

Forge A, Li L. 2000. Apoptotic death of hair cells in mammalian vestibular sensory epithelia. Hear Res 139:97–115.

Forge A, Richardson G. 1993. Freeze fracture analysis of apical membranes in cochlear cultures: differences between basal and apical-coil outer hair cells and effects of neomycin. J Neurocytol 22:854–867.

Forge A, Schacht J. 2000. Aminoglycoside antibiotics. Audiol Neurootol 5:3–22.

Fredelius L, Rask-Andersen H. 1990. The role of macrophages in the disposal of degeneration products within the organ of Corti after acoustic overstimulation. Acta Otolaryngol 109:76–82.

Furness DN, Hackney CM. 1986. Morphological changes to the stereociliary bundles in the guinea pig cochlea after kanamycin treatment. Br J Audiol 20:253–259.

Gale JE, Meyers JR, Periasamy A, Corwin JT. 2002. Survival of bundleless hair cells and subsequent bundle replacement in the bullfrog's saccule. J Neurobiol 50:81–92.

Guan MX, Fischel-Ghodsian N, Attardi G. 2000. A biochemical basis for the inherited susceptibility to aminoglycoside ototoxicity. Hum Mol Genet 9:1787–1793.

Gutell RR. 1994. Collection of small subunit (16S- and 16S-like) ribosomal RNA structures: 1994. Nucleic Acids Res 22:3502–3507.

Harris JA, Cheng AG, Cunningham LL, MacDonald G, Raible DW, Rubel EW. 2003. Neomycin-induced hair cell death and rapid regeneration in the lateral line of zebrafish (Danio rerio). J Assoc Res Otolaryngol 4:219–234.

Hashino E, Marlene S, Salvi RJ. 1997. Lysosomal targeting and accumulation of aminoglycoside antibiotics in sensory hair cells. Brain Res 777:75–85.

Hawkins JE Jr, Lurie MH. 1953. The ototoxicity of dihydrostreptomycin and neomycin in the cat. Ann Otol Rhinol Laryngol 62:1128–1148.

Henderson D, McFadden SL, Liu CC, Hight N, Zheng XY. 1999. The role of antioxidants in protection from impulse noise. Ann N Y Acad Sci 884:368–380.

Hentschel DM, Park KM, Cilenti L, Zervos AS, Drummond I, Bonventre JV. 2005. Acute renal failure in zebrafish: a novel system to study a complex disease. Am J Physiol Renal Physiol 288:F923–929.

Hernandez PP, Moreno V, Olivari FA, Allende ML. 2006. Sub-lethal con-

centrations of waterborne copper are toxic to lateral line neuromasts in zebrafish (Danio rerio). Hear Res 213:1–10.

Heydt JL, Cunningham LL, Rubel EW, Coltrera MD. 2004. Round window gentamicin application: an inner ear hair cell damage protocol for the mouse. Hear Res 192:65–74.

Hiel H, Erre JP, Aurousseau C, Bouali R, Dulon D, Aran JM. 1993. Gentamicin uptake by cochlear hair cells precedes hearing impairment during chronic treatment. Audiology 32:78–87.

Hinshaw HC, Feldman WH. 1945. Streptomycin in the treatment of clinical tuberculosis: a preliminary report. Proc Mayo Clinic 20:313–318.

Hirose K, Hockenbery DM, Rubel EW. 1997. Reactive oxygen species in chick hair cells after gentamicin exposure in vitro. Hear Res 104:1–14.

Hirose K, Westrum LE, Stone JS, Zirpel L, Rubel EW. 1999. Dynamic studies of ototoxicity in mature avian auditory epithelium. Ann N Y Acad Sci 884:389–409.

Hirose K, Westrum LE, Cunningham DE, Rubel EW. 2004. Electron microscopy of degenerative changes in the chick basilar papilla after gentamicin exposure. J Comp Neurol 470:164–180.

Hyde GE, Rubel EW. 1995. Mitochondrial role in hair cell survival after injury. Otolaryngol Head Neck Surg 113:530–540.

Imamura S, Adams JC. 2003. Distribution of gentamicin in the guinea pig inner ear after local or systemic application. J Assoc Res Otolaryngol 4:176–195.

Janas JD, Cotanche DA, Rubel EW. 1995. Avian cochlear hair cell regeneration: stereological analyses of damage and recovery from a single high dose of gentamicin. Hear Res 92:17–29.

Jiang H, Sha SH, Forge A, Schacht J. 2006. Caspase-independent pathways of hair cell death induced by kanamycin in vivo. Cell Death Differ 13:20–30.

Jones JE, Corwin JT. 1996. Regeneration of sensory cells after laser ablation in the lateral line system: hair cell lineage and macrophage behavior revealed by time-lapse video microscopy. J Neurosci 16:649–662.

Jorgensen JM, Flock A. 1973. The ultrastructure of lateral line sense organs in the adult salamander Ambystoma mexicanum. J Neurocytol 2:133–142.

Kaul M, Barbieri CM, Pilch DS. 2005. Defining the basis for the specificity of aminoglycoside-rRNA recognition: a comparative study of drug binding to the A sites of Escherichia coli and human rRNA. J Mol Biol 346:119–134.

Kaus S. 1987. The effect of aminoglycoside antibiotics on the lateral line organ of Aplocheilus lineatus (Cyprinodontidae). Acta Otolaryngol 103: 291–298.

Kelley MW, Talreja DR, Corwin JT. 1995. Replacement of hair cells after laser microbeam irradiation in cultured organs of Corti from embryonic and neonatal mice. J Neurosci 15:3013–3026.

Kita T, Nakagawa T, Kim TS, Iwai K, Takebayashi S, Akaike A, Ito J. 2005. Serofendic acid promotes survival of auditory hair cells and neurons of mice. Neuroreport 16:689–692.

Kopke R, Allen KA, Henderson D, Hoffer M, Frenz D, Van de Water T. 1999. A radical demise. Toxins and trauma share common pathways in hair cell death. Ann N Y Acad Sci 884:171–191.

Kossl M, Richardson GP, Russell IJ. 1990. Stereocilia bundle stiffness: effects of neomycin sulphate, A23187 and concanavalin A. Hear Res 44:217–229.

Kroemer G, Reed JC. 2000. Mitochondrial control of cell death. Nat Med 6:513–519.

Lee KS, Kimura RS. 1994. Ultrastructural changes of the vestibular sensory organs after streptomycin application on the lateral canal. Scan Microsc 8:107–121.

Lee JE, Nakagawa T, Kim TS, Iguchi F, Endo T, Kita T, Murai N, Naito Y, Lee SH, Ito J. 2004. Signaling pathway for apoptosis of vestibular hair cells of mice due to aminoglycosides. Acta Otolaryngol Suppl 551:69–74.

Lenoir M, Puel JL. 1987. Dose-dependent changes in the rat cochlea following aminoglycoside intoxication. II. Histological study. Hear Res 26:199–209.

Lenoir M, Daudet N, Humbert G, Renard N, Gallego M, Pujol R, Eybalin M, Vago P. 1999. Morphological and molecular changes in the inner hair cell region of the rat cochlea after amikacin treatment. J Neurocytol 28:925–937.

Leonova EV, Raphael Y. 1997. Organization of cell junctions and cytoskeleton in the reticular lamina in normal and ototoxically damaged organ of Corti. Hear Res 113:14–28.

Leydig F. 1850. Ueber die Schleimkanale der Knochenfische. Mull Arch Anat Physiol 170–181.

Lopez I, Honrubia V, Lee SC, Schoeman G, Beykirch K. 1997. Quantification of the process of hair cell loss and recovery in the chinchilla crista ampullaris after gentamicin treatment. Int J Dev Neurosci 15:447–461.

Mangiardi DA, McLaughlin-Williamson K, May KE, Messana EP, Mountain DC, Cotanche DA. 2004. Progression of hair cell ejection and molecular markers of apoptosis in the avian cochlea following gentamicin treatment. J Comp Neurol 475:1–18.

Mather M, Rottenberg H. 2001. Polycations induce the release of soluble intermembrane mitochondrial proteins. Biochim Biophys Acta 1503: 357–368.

Matsui JI, Cotanche DA. 2004. Sensory hair cell death and regeneration: two halves of the same equation. Curr Opin Otolaryngol Head Neck Surg 12:418–425.

Matsui JI, Oesterle EC, Stone JS, Rubel EW. 2000. Characterization of damage and regeneration in cultured avian utricles. J Assoc Res Otolaryngol 1:46–63.

Matsui JI, Ogilvie JM, Warchol ME. 2002. Inhibition of caspases prevents ototoxic and ongoing hair cell death. J Neurosci 22:1218–1227.

Matsui JI, Haque A, Huss D, Messana EP, Alosi JA, Roberson DW, Cotanche DA, Dickman JD, Warchol ME. 2003. Caspase inhibitors promote vestibular hair cell survival and function after aminoglycoside treatment in vivo. J Neurosci 23:6111–6122.

Matsui JI, Gale JE, Warchol ME. 2004. Critical signaling events during the aminoglycoside-induced death of sensory hair cells in vitro. J Neurobiol 61:250–266.

McDowell B, Davies S, Forge A. 1989. The effect of gentamicin-induced hair cell loss on the tight junctions of the reticular lamina. Hear Res 40:221–232.

McFadden SL, Ding D, Salvemini D, Salvi RJ. 2003. M40403, a superoxide dismutase mimetic, protects cochlear hair cells from gentamicin, but not cisplatin toxicity. Toxicol Appl Pharmacol 186:46–54.

Metcalfe WK, Kimmel CB, Schabtach E. 1985. Anatomy of the posterior lateral line system in young larvae of the zebrafish. J Comp Neurol 233:377–389.

Minamikawa T, Williams DA, Bowser DN, Nagley P. 1999. Mitochondrial permeability transition and swelling can occur reversibly without inducing cell death in intact human cells. Exp Cell Res 246:26–37.

Murakami SL, Cunningham LL, Werner LA, Bauer E, Pujol R, Raible DW, Rubel EW. 2003. Developmental differences in susceptibility to neomycin-induced hair cell death in the lateral line neuromasts of zebrafish (Danio rerio). Hear Res 186:47–56.

Myrdal SE, Johnson KC, Steyger PS. 2005. Cytoplasmic and intra-nuclear binding of gentamicin does not require endocytosis. Hear Res 204:156–169.

Nakagawa T, Yamane H, Shibata S, Nakai Y. 1997. Gentamicin ototoxicity induced apoptosis of the vestibular hair cells of guinea pigs. Eur Arch Otorhinolaryngol 254:9–14.

Newmeyer DD, Ferguson-Miller S. 2003. Mitochondria: releasing power for life and unleashing the machineries of death. Cell 112:481–490.

Nicolson T. 2005. The genetics of hearing and balance in zebrafish. Annu Rev Genet 39:9–22.

Nicolson T, Rusch A, Friedrich RW, Granato M, Ruppersberg JP, Nusslein-Volhard C. 1998. Genetic analysis of vertebrate sensory hair cell mechanosensation: the zebrafish circler mutants. Neuron 20:271–283.

Nicotera TM, Hu BH, Henderson D. 2003. The caspase pathway in noise-induced apoptosis of the chinchilla cochlea. J Assoc Res Otolaryngol 4:466–477.

Park JC, Cohen GM. 1984. Further observations of vestibular ototoxicity in the chick: effects of streptomycin on the ampullary sensory epithelium. Am J Otolaryngol 5:387–393.

Peng TI, Jou MJ. 2004. Mitochondrial swelling and generation of reactive oxygen species induced by photoirradiation are heterogeneously distributed. Ann N Y Acad Sci 1011:112–122.

Pickles JO. 2004. Mutation in mitochondrial DNA as a cause of presbyacusis. Audiol Neurootol 9:23–33.

Pickles JL, Rouse GW. 1991. Effects of streptomycin on development of the apical structures of hair cells in the chick basilar papilla. Hear Res 55:244–254.

Pickles JO, Comis SD, Osborne MP. 1987. The effect of chronic application of kanamycin on stereocilia and their tip links in hair cells of the guinea pig cochlea. Hear Res 29:237–244.

Pirvola U, Xing-Qun L, Virkkala J, Saarma M, Murakata C, Camoratto AM, Walton KM, Ylikoski J. 2000. Rescue of hearing, auditory hair cells, and neurons by CEP-1347/KT7515, an inhibitor of c-Jun N-terminal kinase activation. J Neurosci 20:43–50.

Popper AN, Fay RR. 1999. The auditory periphery in fishes. Fay RR, Popper AN, editors. New York: Springer. p 43–100.

Poss KD, Keating MT, Nechiporuk A. 2003. Tales of regeneration in zebrafish. Dev Dyn 226:202–210.

Priuska EM, Schacht J. 1995. Formation of free radicals by gentamicin and iron and evidence for an iron/gentamicin complex. Biochem Pharmacol 50:1749–1752.

Pujol R, Puel JL. 1999. Excitotoxicity, synaptic repair, and functional recovery in the mammalian cochlea: a review of recent findings. Ann N Y Acad Sci 884:249–254.

Raible DW, Kruse GJ. 2000. Organization of the lateral line system in embryonic zebrafish. J Comp Neurol 421:189–198.

Rasband WS. 1997–2006. ImageJ, US National Institutes of Health, Bethesda, MD; http://rsb.info.nih.gov/ij/

Raphael Y, Athey BD, Wang Y, Hawkins JE Jr. 1993. Structure of the reticular lamina and repair after noise injury. Rev Laryngol Otol Rhinol (Bord) 114:171–175.

Recht MI, Douthwaite S, Puglisi JD. 1999. Basis for prokaryotic specificity of action of aminoglycoside antibiotics. EMBO J 18:3133–3138.

Redd MJ, Cooper L, Wood W, Stramer B, Martin P. 2004. Wound healing and inflammation: embryos reveal the way to perfect repair. Philos Trans R Soc Lond B Biol Sci 359:777–784.

Richardson GP, Russell IJ. 1991. Cochlear cultures as a model system for studying aminoglycoside induced ototoxicity. Hear Res 53:293–311.

Rybak LP, Whitworth CA. 2005. Ototoxicity: therapeutic opportunities. Drug Discov Today 10:1313–1321.

Sandoval RM, Molitoris BA. 2004. Gentamicin traffics retrograde through the secretory pathway and is released in the cytosol via the endoplasmic reticulum. Am J Physiol Renal Physiol 286:F617–624.

Santos F, MacDonald G, Rubel EW, Raible DW. 2006. Lateral line hair cell maturation is a determinant of aminoglycoside susceptibility in zebrafish (Danio rerio). Hear Res 213:25–33.

Schacht J. 1999. Antioxidant therapy attenuates aminoglycoside-induced hearing loss. Ann N Y Acad Sci 884:125–130.

Sha SH, Schacht J. 1999. Stimulation of free radical formation by aminoglycoside antibiotics. Hear Res 128:112–118.

Sha SH, Taylor R, Forge A, Schacht J. 2001. Differential vulnerability of basal and apical hair cells is based on intrinsic susceptibility to free radicals. Hear Res 155:1–8.

Sidi S, Busch-Nentwich E, Friedrich R, Schoenberger U, Nicolson T. 2004. Gemini encodes a zebrafish L-type calcium channel that localizes at sensory hair cell ribbon synapses. J Neurosci 24:4213–4223.

Sobkowicz HM, Bereman B, Rose JE. 1975. Organotypic development of the organ of Corti in culture. J Neurocytol 4:543–572.

Song J, Yan HY, Popper AN. 1995. Damage and recovery of hair cells in fish canal (but not superficial) neuromasts after gentamicin exposure. Hear Res 91:63–71.

Steyger PS, Peters SL, Rehling J, Hordichok A, Dai CF. 2003. Uptake of gentamicin by bullfrog saccular hair cells in vitro. J Assoc Res Otolaryngol 4:565–578.

Stone LS. 1933. The development of lateral-line sense organs in amphibians observed in living and vital-stained preparations. J Comp Neurol 57:507–540.

Sun H, Hashino E, Ding DL, Salvi RJ. 2001. Reversible and irreversible damage to cochlear afferent neurons by kainic acid excitotoxicity. J Comp Neurol 430:172–81.

Tachibana M, Morioka H, Machino M, Mizukoshi O. 1985. Binding sites of an aminoglycoside in the cochlea examined by immunocytochemistry. Histochemistry 83:237–240.

Takumida M, Bagger-Sjoback D, Harada Y, Lim D, Wersall J. 1989. Sensory hair fusion and glycocalyx changes following gentamicin exposure in the guinea pig vestibular organs. Acta Otolaryngol 107:39–47.

Takumida M, Anniko M, Shimizu A, Watanabe H. 2003. Neuroprotection of vestibular sensory cells from gentamicin ototoxicity obtained using nitric oxide synthase inhibitors, reactive oxygen species scavengers, brain-derived neurotrophic factors and calpain inhibitors. Acta Otolaryngol 123:8–13.

Tran Ba Huy P, Bernard P, Schacht J. 1986. Kinetics of gentamicin uptake and release in the rat. Comparison of inner ear tissues and fluids with other organs. J Clin Invest 77:1492–1500.

Vago P, Humbert G, Lenoir M. 1998. Amikacin intoxication induces apoptosis and cell proliferation in rat organ of Corti. Neuroreport 9:431–436.

Vakulenko SB, Mobashery S. 2003. Versatility of aminoglycosides and prospects for their future. Clin Microbiol Rev 16:430–450.

Vander Heiden MG, Chandel NS, Williamson EK, Schumacker PT, Thompson CB. 1997. Bcl-xL regulates the membrane potential and volume homeostasis of mitochondria. Cell 91:627–637.

Vicens Q, Westhof E. 2003. Molecular recognition of aminoglycoside antibiotics by ribosomal RNA and resistance enzymes: an analysis of x-ray crystal structures. Biopolymers 70:42–57.

Wagner N, Caye-Thomasen P, Laurell G, Bagger-Sjoback D, Thomsen J. 2005. Cochlear hair cell loss in single-dose versus continuous round window administration of gentamicin. Acta Otolaryngol 125:340–345.

Wallace D. 2005. A mitochondrial paradigm of metabolic and degenerative diseases, aging, and cancer: a dawn of evolutionary medicine. Annu Rev Genet 39:357–407.

Wang J, Van De Water TR, Bonny C, de Ribaupierre F, Puel JL, Zine A. 2003. A peptide inhibitor of c-Jun N-terminal kinase protects against both aminoglycoside and acoustic trauma-induced auditory hair cell death and hearing loss. J Neurosci 23:8596–8607.

Webb JF, Shirey JE. 2003. Postembryonic development of the cranial lateral line canals and neuromasts in zebrafish. Dev Dyn 228:370–385.

Weil M, Jacobson MD, Coles HS, Davies TJ, Gardner RL, Raff KD, Raff MC. 1996. Constitutive expression of the machinery for programmed cell death. J Cell Biol 133:1053–1059.

Weisleder P, Rubel EW. 1992. Hair cell regeneration in the avian vestibular epithelium. Exp Neurol 115:2–6.

Wersaell J, Flock A. 1965. Functional anatomy of the vestibular and lateral line organs. Contrib Sens Physiol 14:39–61.

Wersall J, Hawkins JE Jr. 1962. The vestibular sensory epithelia in the cat labyrinth and their reactions in chronic streptomycin intoxication. Acta Otolaryngol 54:1–23.

Westerfield M. 1995. The zebrafish book. Eugene: University of Oregon Press.

Wilhelm JM, Jessop JJ, Pettitt SE. 1978. Aminoglycoside antibiotics and eukaryotic protein synthesis: stimulation of errors in the translation of natural messengers in extracts of cultured human cells. Biochemistry 17:1149–1153.

Williams JA, Holder N. 2000. Cell turnover in neuromasts of zebrafish larvae. Hear Res 143:171–181.

Williams SE, Zenner HP, Schacht J. 1987. Three molecular steps of aminoglycoside ototoxicity demonstrated in outer hair cells. Hear Res 30:11–18.

Yan Q, Li X, Faye G, Guan MX. 2005. Mutations in MTO2 related to tRNA modification impair mitochondrial gene expression and protein synthesis in the presence of a paromomycin resistance mutation in mitochondrial 15 S rRNA. J Biol Chem 280:29151–29157.

Ylikoski J. 1974. Guinea-pig hair cell pathology from ototoxic antibiotics. Acta Otolaryngol Suppl 326:5–22.

Ylikoski J, Xing-Qun L, Virkkala J, Pirvola U. 2002. Blockade of c-Jun N-terminal kinase pathway attenuates gentamicin-induced cochlear and vestibular hair cell death. Hear Res 166:33–43.

Zhao H, Li R, Wang Q, Yan Q, Deng JH, Han D, Bai Y, Young WY, Guan MX. 2004. Maternally inherited aminoglycoside-induced and nonsyndromic deafness is associated with the novel C1494T mutation in the mitochondrial 12S rRNA gene in a large Chinese family. Am J Hum Genet. 74:139–152.